

NMR Conformation of (–)-β-D-Aristeromycin and Its 2'-Deoxy and 3'-Deoxy Counterparts in Aqueous Solution

C. Thibaudeau,[†] A. Kumar,[†] S. Bekiroglu,[†] A. Matsuda,[‡] V. E. Marquez,[§] and J. Chattopadhyaya^{*†}

Department of Bioorganic Chemistry, Box 581, Biomedical Center, University of Uppsala, S-751 23 Uppsala, Sweden, Laboratory of Medicinal Chemistry, DPT, DCT, National Cancer Institute, NIH, Bethesda, Maryland 20892, and Faculty of Pharmaceutical Sciences, Hokkaido University, Sapporo 060, Japan

Received February 26, 1998

The solution conformations of aristeromycin (**1**), 2'-deoxyaristeromycin (**2**), and 3'-deoxyaristeromycin (**3**) have been determined from an integrated analysis of X-ray (for **1** only), NMR data (i.e., $^3J_{\text{HH}}$ coupling constants), and ab initio calculations. One-dimensional NOE difference experiments showed that the adenin-9-yl ring in **1** and **2** is involved in a $\sim 50\%$ *syn* \rightleftharpoons $\sim 50\%$ *anti* equilibrium around the C-glycosyl torsion angle, whereas an anti orientation ($\chi = -113^\circ$) is found in the X-ray crystal structure of **1**. The preferred conformation around the γ torsion angle is γ^t both in solution for **1–3** and in the solid state (for **1** only). The plots of energy as a function of the phase angle of pseudorotation (Figure 2) for the structures optimized by ab initio calculations (HF/3-21G*) show that there are two major wells of low energy conformers for **1–3**, supporting the two-state North-type \rightleftharpoons South/West-type equilibrium of the constituent cyclopentane rings in **1–3**. The ab initio calculations suggested that the South/West-type conformers are more stable than the North-type forms for **1** [$\Delta E(120^\circ < P < 240^\circ) - (330^\circ < P < 30^\circ) \sim 10$ kcal/mol], for **2** [$\Delta E(210^\circ < P < 240^\circ) - (330^\circ < P < 60^\circ) \sim 4$ kcal/mol] and for **3** [$\Delta E(P = 240^\circ) - (330^\circ < P < 0^\circ) \sim 6$ kcal/mol]. Newly developed A and B sets of parameters correlating the H–C–C–H torsions to the endocyclic torsions based on the ab initio optimized structures of **1–3** have been subsequently used to interpret the time-averaged $^3J_{\text{HH}}$ couplings using the program PSEUROT. The discrepancy found between the X-ray crystal structure ($P = 89^\circ$, $\Psi_m = 41^\circ$) of aristeromycin (**1**) and its structure calculated by NMR-PSEUROT conformational analysis ($35^\circ < P [{}^3_4\text{T} - {}^0_4\text{T}] < 65^\circ$, $35^\circ < \Psi_m < 45^\circ$) \rightleftharpoons ($128^\circ < P [{}_1\text{E}] < 131^\circ$, $34^\circ < \Psi_m < 36^\circ$) based on observed $^3J_{\text{HH}}$ couplings in aqueous solution, as well as the relatively high error in the NMR-PSEUROT analyses for **1–3** [$\Delta J_{\text{max}} \leq 1.6$ Hz (i.e., maximal difference between experimental and PSEUROT-calculated $^3J_{\text{HH}}$) and root mean square (rms) error ≤ 0.7 Hz] prompted us to reparametrize the Karplus equation implemented in the PSEUROT program by using torsion angles derived from solid-state geometries of conformationally constrained nucleosides and their corresponding experimental $^3J_{\text{HH}}$. The precision of our reparametrized Karplus-type equation (rms error = 0.40 Hz) became comparable to that expected for the standard Haasnoot–Altona Karplus (0.48 Hz) equation. The results of the PSEUROT analyses performed with the standard Haasnoot–Altona Karplus equation are also very comparable in terms of geometry with those based on our reparametrized equation (eq 4). Both series of PSEUROT analyses suggest that the predominant conformation of the cyclopentane ring in **1–3** is defined by $128^\circ < P < 140^\circ$ for **1**, $105^\circ < P < 116^\circ$ for **2**, and $118^\circ < P < 127^\circ$ for **3**, with the puckering amplitude in the range from 34° to 40° for **1–3**. However, PSEUROT analyses based on our Karplus equation produced a smaller rms error by ≤ 0.14 Hz and ΔJ_{max} error by ≤ 0.5 Hz than those performed with the standard Haasnoot–Altona equation. This work therefore highlights two important points: (i) the solution- and the solid-state structures of aristeromycin (**1**) are indeed different, and (ii) the close similarity of geometries derived from Haasnoot–Altona's equation or from our Karplus equation suggest that the solution structures for **1–3** are correctly defined.

Introduction

Aristeromycin was first isolated from the culture broth of *Streptomyces citricolor* by Kusaka et al.,¹ and shown to possess in vitro and in vivo antibiotic activity against *Xanthomonas oryzae* and *Pycularia oryzae*. The chemi-

cal and enzymatic vulnerability characteristic of the glycosyl bond of natural nucleosides has inspired the synthesis of a wide gamut of carbocyclic nucleosides^{2a} in which a cyclopentane ring replaces the ribose moiety. However, these more stable carbocyclic nucleosides are generally less potent^{2b} than their natural counterparts. This could be attributed to the more flexible nature of the cyclopentane ring where both anomeric and gauche

* To whom correspondence should be addressed. Fax: +46 18 554495. E-mail: jyoti@bioorgchem.uu.se. Web site: http://bioorgchem.boc.uu.se.

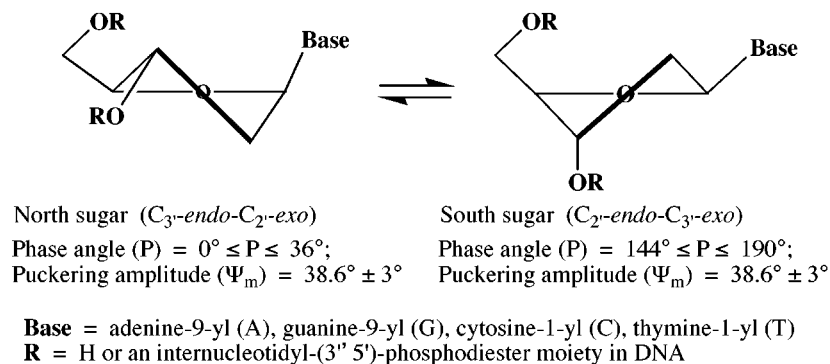
[†] University of Uppsala.

[‡] Hokkaido University.

[§] National Cancer Institute.

(1) Kusaka, T.; Yamamoto, H.; Shibata, M.; Muroi, M.; Kishi, T. and Mizuno, K. *J. Antibiot. (Tokyo)* **1968**, *21*, 255.

(2) (a) Marquez, V. E.; Lim, M. I. *Med. Res. Rev.* **1986**, *6*, 1. (b) Marquez, V. E. *Carbocyclic Nucleosides in Advances in Antiviral Drug Design*; De Clercq, E., Ed.; JAI Press, Inc.: Greenwich, CT, 1997; Vol. 2.

Scheme 1. Two-State N \rightleftharpoons S Pseudorotational Equilibrium in Nucleosides and Nucleotides

ingam's phase angle of pseudorotation (P), which provides information about the most puckered region of the ring, and maximum puckering amplitude (Ψ_m), which indicates the extent of deviation from planarity. P and Ψ_m can be simply calculated from the set of five endocyclic torsion angles.¹³

(II) The Two-State North (N, $0^\circ < P_N < 36^\circ$) \rightleftharpoons South (S, $144^\circ < P_S < 190^\circ$) Pseudorotational Equilibrium for the Pentofuranose Moiety of Natural Nucleosides in Aqueous Solution. A perusal¹⁴ of the X-ray crystal structures of nucleos(t)ides available showed that P s of the constituent pentofuranose moieties are not evenly distributed over the entire pseudorotation cycle (Figure 1); instead, they are clustered in two regions referred to as North (N, C_2' -exo- C_3' -endo, $0^\circ < P_N < 36^\circ$) and South (S, C_2' -endo- C_3' -exo, $144^\circ < P_S < 180^\circ$). Thus, the X-ray data for nucleos(t)ides suggested that in solution there would be a dynamic two-state North \rightleftharpoons South equilibrium (Scheme 1) for the pentofuranose moieties.

The hypothesis of two-state model in solution has been experimentally confirmed by the NMR observations of two distinctly identifiable and dynamically interconverting N and S conformations of the sugar moieties in nucleosides as well as in oligonucleotides where B \rightleftharpoons Z DNA,^{15a,b} A \rightleftharpoons Z RNA,^{15c,d} or A-form \rightleftharpoons B-form lariat RNA^{15e,f} transitions are observed. On the basis of the validity of the two-state model, we have shown³ that the conformation of the sugar in nucleos(t)ides is driven by the balance of stereoelectronic and steric effects. We found^{3n,q-s} that the strength of the stereoelectronic forces is dictated by protonated/neutral/deprotonated state of the nucleobase, which is in turn dictated by the pH (pD in NMR studies) of the medium. For β -D-2',3'-dideoxy-,^{3r} β -D-2'-deoxy-³ⁿ, and β -D-ribo-*N*-nucleosides,³ⁿ β -D-ribo-*C*-nucleosides,^{3q} and α -D-2',3'-dideoxyribo-^{3r} and α -D-2'-deoxyribo-*N*-nucleosides^{3s} the pDs at the inflection points of the sigmoidal plots (ΔG° of N \rightleftharpoons S equilibria vs pD) correspond to the pK_as of the nucleobases. These results confirmed that the pentofuranose moiety in nucleos(t)ides is indeed engaged in a two-state equilibrium in D₂O solution.

On the other hand, the substitution of O4' by a methylene group in carbocyclic nucleosides results in the cancellation of the anomeric effect³ of the nucleobase and the gauche effects³ of the (O4'-C1'-C2'-O2') and/or (O4'-C4'-C3'-O3') fragments. Hence, we assumed that the absence of the gauche and anomeric effects is likely

to result in a relatively low-energy barrier amongst various pseudorotational forms of the cyclopentane moiety in carbocyclic nucleosides, and this might prevent it to take up any preferential conformation compared to the pentofuranose counterparts. This assumption is supported by the various forms of pucker found for the cyclopentanyl moieties in the X-ray crystal structures of various monomeric carbocyclic nucleosides.⁷⁻¹⁰

That the cyclopentane moiety can indeed assume the conformation of neighboring nucleotides in modified DNA duplexes,¹¹ as expected from the absence of anomeric and gauche effects, is also evident from the various puckering modes observed for the cyclopentane moieties in the four 7'- α -methylcarbocyclic (T*) and 6'- α -hydroxycarbocyclic (T⁶) thymidine residues in the X-ray crystal structures of d(CGCGAAT*^T*CGCG)₂ and d(CGCGAAT^{T6}CGCG)₂, respectively. Hence, it was important, at the outset, to establish the energetics of interconversions amongst various conformers of the cyclopentane moiety in carbocyclic nucleosides.

(III) Determination of the Solution Structure of Carbocyclic Nucleosides 1-3 through the Interpretation of $^3J_{\text{HH}}$ Coupling Constants with the PSEUROT Program. The summary of the methodology used in the elucidation of the conformation of 1-3 (Chart 1) using the integrated X-ray, NMR, and ab initio approach is outlined in Scheme 2 as fully described below.

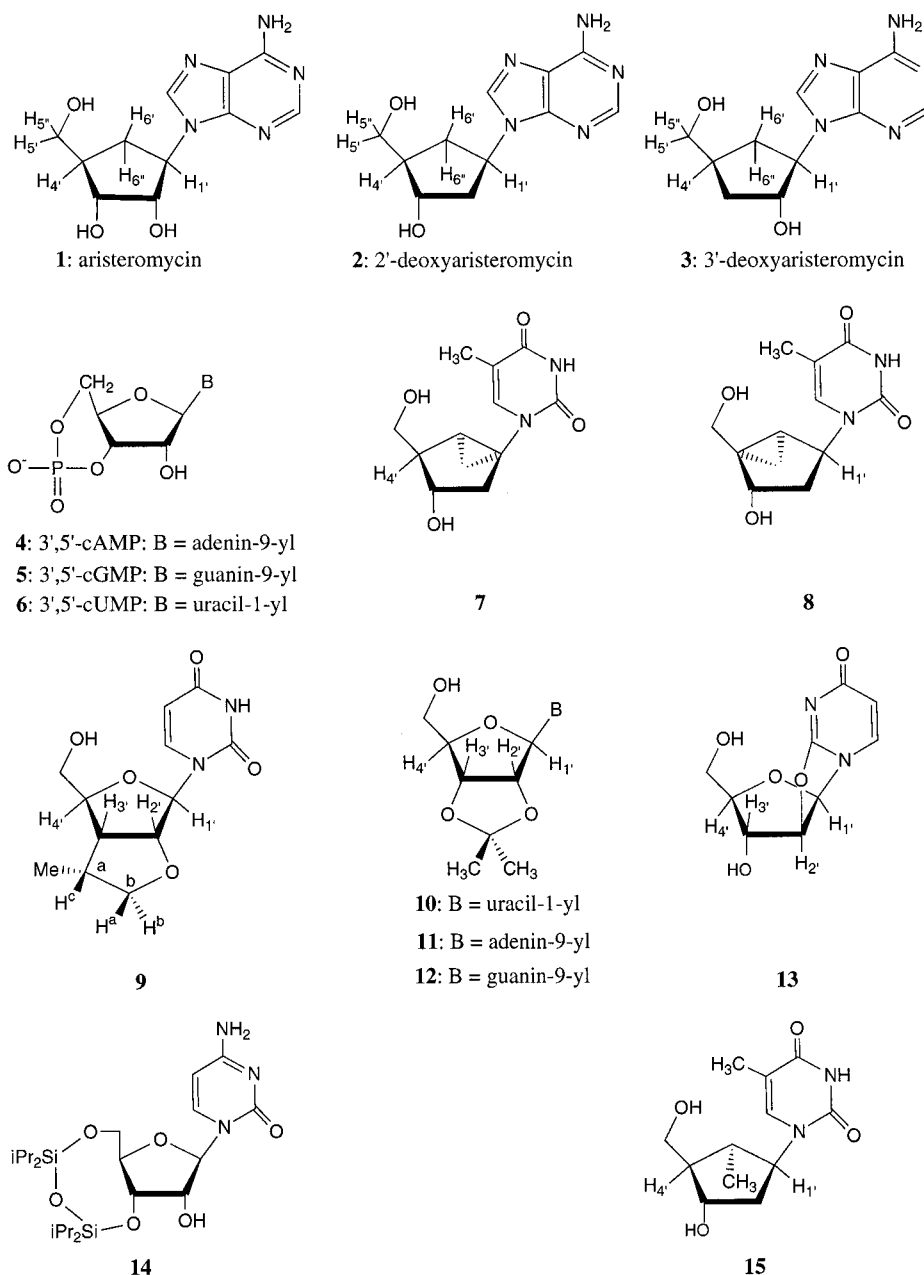
(A) Comparison of the Cyclopentane Conformation in 1-3 at pD 2 and 7 by ^1H NMR Studies. One-dimensional ^1H spectra of 1-3 (5 mM D₂O solutions) were recorded at 500 MHz throughout the 278-358 K temperature range at pD \sim 2.0 and \sim 7.0 to examine the effect of aglycone protonation on the drive of the pseudorotational equilibrium of the cyclopentane moieties in 1-3. All $^3J_{\text{HH}}$ have been extracted from 1D spectra and simulated using the DAISY program¹⁶ (Table 1).

We have previously shown that the free-energy (ΔG°) of the protonation \rightleftharpoons deprotonation equilibrium drives the two-state N \rightleftharpoons S equilibrium of the furanose moiety in *N*-^{3n,r,s} and *C*-nucleosides^{3q} through the anomeric effect. Therefore, the electronic nature of the aglycon is reflected in the ΔG° of the N \rightleftharpoons S equilibrium of the constituent pentofuranose moiety. In fact, the pK_a value of the constituent nucleobase can be calculated either from a pD-dependent change of ΔG° in the N \rightleftharpoons S equilibrium or from pD-dependent chemical shift plots.

Hence, we have examined the $^3J_{\text{HH}}$ of 1-3 at pD \sim 2 and \sim 7 in the 278-358 K range to see whether the protonation \rightleftharpoons deprotonation equilibrium of the adenine-9-yl base also drives the conformational equilibrium of their constituent cyclopentane moieties. As expected,

(13) Altona, C.; Sundaralingam, M. *J. Am. Chem. Soc.* **1972**, *94*, 8205; **1973**, *95*, 2333.

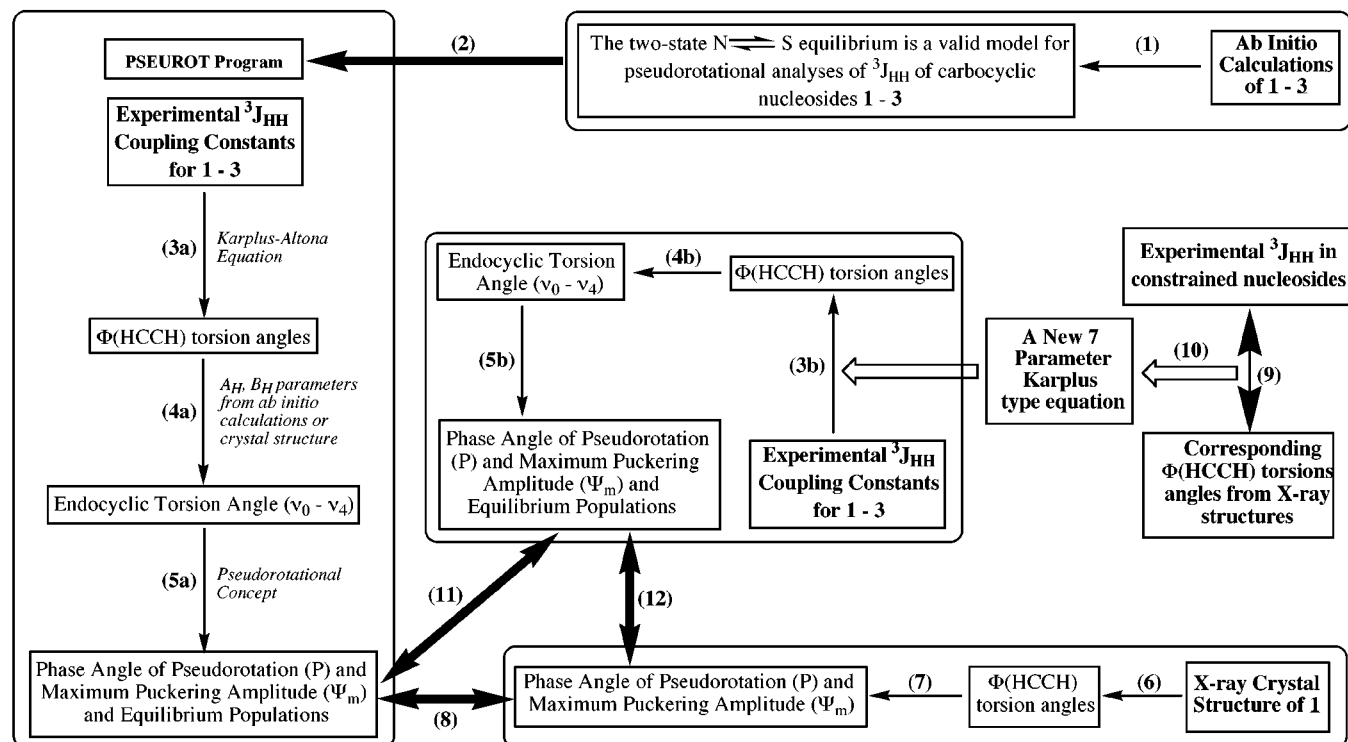
Chart 1



temperature-dependent $^3J_{\text{HH}}$ values are virtually unchanged from acidic to neutral *pD*s (at most ± 0.15 Hz, Table 1). This provides additional evidence in support of the role of the anomeric effect³ in *N*- and *C*-nucleosides in one hand, and on the other, it shows that the electronic character of the nucleobase (i.e., protonated or deprotonated) in carbocyclic nucleosides **1–3** does not have any effect on the drive of the conformation of their cyclopentane moieties.

(B) The Proof of the Validity of the Two-State N-Type \rightleftharpoons S (or W)-Type Equilibrium Model for the Cyclopentane Ring in Carbocyclic Nucleosides **1–3 by ab Initio Calculations (Step 1 in Scheme 2).** For pentofuranosyl nucleosides, Altona et al. showed that experimental $^3J_{\text{HH}}$ values can be interpreted in terms of a two-state $\text{N} \rightleftharpoons \text{S}$ pseudorotational equilibrium of the sugar moiety, which could be determined with the help of the computer program PSEUROT.¹⁷ This program calculates the best fit of the conformational parameters defining the two-state pseudorotational equilibrium to

the experimental time-averaged $^3J_{\text{HH}}$ values. In order to be able to use the PSEUROT program for the conformational analysis of **1–3**, we have examined the validity of the hypothesis of the two-state N-type \rightleftharpoons S-type equilibrium for the cyclopentane ring in these carbocyclic nucleosides by ab initio calculations. A set of ab initio (HF/3-21G*) calculations (Figure 2) with the GAUSSIAN 94 program¹⁸ for **1–3** has been performed, in which *P* of the cyclopentane moiety was incremented from 0° to 330° in 30° steps by constraining two endocyclic torsions (ν_0 and ν_4) during the optimizations (this is necessary to produce a fixed *P* during optimization). Ψ_m was kept fixed to 41° as found in the crystal structure of **1**. The plots of energy as a function of *P* (Figure 2) show that for **1–3** there are indeed two major energy wells: (i) The South/West-type conformers ($120^\circ < P < 240^\circ$) are preferred over the North-type ($330^\circ < P < 30^\circ$) geometries for aristeromycin (**1**) by ~ 10 kcal/mol. (ii) The South-type or West-type conformers ($210^\circ < P < 240^\circ$) are energetically preferred by ~ 3 kcal/mol over the

Scheme 2. Iterative Structure Elucidation of Carbocyclic Nucleosides 1–3 Using NMR-PSEUROT and ab Initio Calculations and Comparisons

Table 1. Experimental $^3J_{\text{HH}}$ Coupling Constants^a at Two Extreme Temperatures^b for Aristeromycin (1), 2'-Deoxyaristeromycin (2), and 3'-Deoxyaristeromycin (3)

	pD	T (K)	$^3J_{1'2'}$	$^3J_{1'2''}$	$^3J_{2'3'}$	$^3J_{2'3''}$	$^3J_{3'4'}$	$^3J_{3'4''}$	$^3J_{6'1'}$	$^3J_{6'1''}$	$^3J_{4'6'}$	$^3J_{4'6''}$	$^3J_{4'5'}$	$^3J_{4'5''}$
aristeromycin (1)	1.8	278	9.4		5.7		3.2		10.9	8.3	8.6	8.8	6.5	6.4
		358	8.8		5.9		3.9		10.7	8.2	8.9	8.6	6.3	6.3
	7.0	278	9.5		5.7		3.2		10.9	8.2	8.9	8.7	6.5	6.3
		358	8.8		5.9		3.9		10.7	8.1	9.1	8.6	6.3	6.2
2'-deoxyaristeromycin (2)	2.0	278	9.1	8.2	7.3		4.0	5.3	9.8	7.6	10.2	7.7	5.8	6.7
		358	9.0	8.2	7.2		4.1	5.4	9.7	7.6	9.9	7.8	6.0	6.5
	6.9	278	9.3	8.0	7.3		3.9	5.3	9.7	7.6	10.2	7.6	5.8	6.6
		358	9.0	8.1	7.2		4.1	5.4	9.7	7.6	9.9	7.8	6.0	6.5
3'-deoxyaristeromycin (3)	1.8	278	8.1		8.3	7.5	6.1	9.9	11.5	7.7	9.7	7.6	6.6	6.6
		358	7.6		8.3	6.9	6.4	9.4	11.0	7.8	9.3	7.7	6.4	6.4
	7.1	278	8.1		8.5	7.2	6.2	9.9	11.5	7.7	9.8	7.5	6.5	6.5
		358	7.6		8.3	6.9	6.5	9.7	11.0	7.8	9.5	7.7	6.7	6.5

^a The coupling constants have been extracted from only 1D ^1H NMR spectra recorded at 500.13 MHz in D_2O solution. They have been simulated using DAISY¹⁶ program. ^b Here, we only report $^3J_{\text{HH}}$ at only two extreme temperatures. However, for the pseudorotational analyses, we have also used seven intermediate temperatures in 10 K steps.

North-type pseudorotamers ($60^\circ < P < 330^\circ$) for 2'-deoxyaristeromycin (2). (iii) The west-type conformers ($P = 240^\circ$) are more stable than the N-type forms ($330^\circ < P < 360^\circ$) by ~ 6 kcal/mol for 3'-deoxyaristeromycin (3). Therefore, these energy plots (Figure 2) suggest that it is possible to use the PSEUROT program to estimate the conformational properties of the cyclopentane ring in 1–3, based on the assumption of a two-state equilibrium

in solution, as in the case of the pentofuranose moiety in natural nucleosides.^{13–15} However, the energy plots (Figure 2) qualitatively would predict that the S/W-type cyclopentane pseudorotamers are clearly predominant.

The presence of the two-state equilibrium for 1–3 can also be qualitatively understood experimentally by examining a plot of $^3J_{3'4'}$ vs $^3J_{1'2'}$ [section III D (i) and Figure 3]. These plots show that the conformation of the cyclopentane ring in 1–3 is strongly biased ($\geq 90\%$) and that the population of these major conformers is only slightly reduced when the temperature is increased. Since it is possible to fit a straight line through the temperature-dependent experimental data, it implies that the cyclopentane ring in 1–3 is indeed involved in a conformational equilibrium between two species.

(C) Pseudorotational Analyses of $^3J_{\text{HH}}$ Couplings for 1–3 Using the PSEUROT Program (Steps 2, and 3a – 5a in Scheme 2) and the Original Set of Altona's Parameters for the Karplus-Type Equ-

(14) de Leeuw, H. P. M.; Haasnoot, C. A. G.; Altona, C. *Isr. J. Chem.* **1980**, *20*, 108.

(15) (a) Feigon, J.; Wang, A. H.-J.; van der Marel, G. A.; van Boom, J. H.; Rich, A. *Nucl. Acids Res.* **1984**, *12*, 1243. (b) Tran-Dinh, S.; Taboury, J.; Neumann, J.-M.; Huynh-Dinh, T.; Genissel, B.; Laglois d'Estaintot, B.; Igolen, J. *Biochemistry* **1984**, *23*, 1362. (c) Davis, P. W.; Hall, K.; Cruz, P.; Tinoco, I.; Neilson, T. *Nucl. Acids Res.* **1986**, *14*, 1279. (d) Davis, P. W.; Adamiak, R. W.; Tinoco, I. *Biopolymers* **1990**, *29*, 109. (e) Agback, P.; Sandstrom, A.; Yamakage, S.-I.; Sund, C.; Glemarec, C.; Chattopadhyaya, J. *J. Biochem. Biophys. Methods* **1993**, *27*, 229. (f) Agback, P.; Glemarec, C.; Yin, L.; Sandstrom, A.; Plavec, J.; Sund, C.; Yamakage, S.-I.; Wiswanadham, G.; Rousse, B.; Puri, N.; Chattopadhyaya, J. *Tetrahedron Lett.* **1993**, *34*, 3929.

(16) DAISY, Spin Simulation Program, was provided by Bruker.

Table 2. *A, B* Parameters^a for the Correlation of Endocyclic C–C–C–C Torsions with H–C–C–H Torsions from Constrained Sugar Geometries Optimized Using GAUSSIAN Program at HF/3-21G* Level for Aristeromycin (1), 2'-Deoxyaristeromycin (2), and 3'-Deoxyaristeromycin (3)

Φ_{HH}	aristeromycin (1)		2'-deoxyaristeromycin (2)		3'-deoxyaristeromycin (3)	
	<i>A</i> (σ)	<i>B</i> (σ)	<i>A</i> (σ)	<i>B</i> (σ)	<i>A</i> (σ)	<i>B</i> (σ)
$\Phi_{1'2'}$	1.09 (0.01)	124.3 (0.3)	1.16 (0.01)	119.3 (0.2)	1.13 (0.02)	122.0 (0.5)
$\Phi_{1'2''}$			1.16 (0.01)	-1.1 (0.3)		
$\Phi_{2'3'}$	1.13 (0.01)	0.4 (0.4)	1.17 (0.01)	0.2 (0.4)	1.15 (0.02)	-2.0 (0.5)
$\Phi_{2'3''}$					1.14 (0.02)	-120.3 (0.4)
$\Phi_{2''3'}$			1.17 (0.01)	121.0 (0.2)		
$\Phi_{3'4'}$	1.09 (0.01)	-125.9 (0.4)	1.12 (0.01)	-122.2 (0.3)	1.12 (0.02)	-122.5 (0.4)
$\Phi_{3'4''}$					1.12 (0.02)	-2.5 (0.5)
$\Phi_{6'1'}$	1.11 (0.01)	-122.7 (0.4)	1.14 (0.01)	-120.5 (0.3)	1.14 (0.02)	-122.4 (0.5)
$\Phi_{6'1''}$	1.09 (0.01)	-3.6 (0.3)	1.13 (0.01)	-0.2 (0.3)	1.13 (0.01)	-3.8 (0.3)
$\Phi_{4'6'}$	1.10 (0.01)	123.8 (0.4)	1.14 (0.01)	123.4 (0.3)	1.13 (0.02)	121.3 (0.6)
$\Phi_{4'6''}$	1.09 (0.01)	3.6 (0.3)	1.14 (0.01)	1.9 (0.2)	1.13 (0.02)	1.9 (0.4)

^a All torsion angle values are given in degrees [see text, section III C (ii)]. *A* and *B* values designate the slopes and intercepts of the best straight lines through the plots of H–C–C–H torsions as a function of the corresponding C–C–C–C torsions in **1–3** (see Figure 4). The standard deviations are indicated in parentheses.

tion. Since the above ab initio calculations and qualitative analysis of $^3J_{\text{HH}}$ couplings support a two-state equilibrium for **1–3**, we have used the two-state model incorporated in the PSEUROT program (version 3B)¹⁷ to interpret the temperature-dependent experimental $^3J_{\text{HH}}$ values. The procedure involved in PSEUROT to translate experimental $^3J_{\text{HH}}$ couplings into the parameters necessary to describe the N-type \rightleftharpoons S-type pseudorotational equilibrium [i.e., P_{N} and $\Psi_{\text{m}}(\text{N})$, P_{S} and $\Psi_{\text{m}}(\text{S})$] and the mole fraction of either N- or S-type conformer] is based on three translational steps (Scheme 2, steps 3a–5a). The experimental $^3J_{\text{HH}}$ are compared to ones calculated by PSEUROT using the values of *P* and Ψ_{m} of both N- and S-type conformers and their respective populations defined in the user's input. In the following iterative steps, random changes are made in *P* and Ψ_{m} values, as well as in the populations depending on the user's input, which defines the parameters that are to be optimized or kept fixed. The discrepancy between experimental and calculated $^3J_{\text{HH}}$ is monitored and optimized. When the best fit is found, the optimized geometries of the N and S conformers and their populations are determined together with the error analysis, which shows both individual differences between experimental and calculated $^3J_{\text{HH}}$ (ΔJ_{max}) and the overall root mean square (rms) error.

(i) The Karplus-Type Equation To Translate Vicinal $^3J_{\text{HH}}$ Couplings into $\Phi_{\text{H-C-C-H}}$ Torsion Angles (Step 3a in Scheme 2). Using a Karplus-type equation, $^3J_{\text{HH}}$ couplings, either for the N- or S-type conformer, are translated into the corresponding $\Phi_{\text{H-C-C-H}}$ torsion angles. In version 3B^{17a} of PSEUROT, the Karplus-type equation has been parametrized by Haasnoot–Altona,^{17b} and it has the following form (eq 1):

$$^3J_{\text{HH}} = P_1 \cos^2 \Phi_{\text{HH}} + P_2 \cos \Phi_{\text{HH}} + P_3 + \sum_{i=1-4} \Delta\chi_{i(\text{g})} [P_4 + P_5 \cos^2 (\zeta_i \Phi_{\text{HH}} + P_6 |\Delta\chi_{i(\text{g})})]$$

where

$$\Delta\chi_{i(\text{g})} = \Delta\chi_{i(\alpha)} - P_7 \sum_{j=1-n} \Delta\chi_j (\beta \text{ substituent}) \quad (1)$$

The summation term takes into account substituent effects, which are assumed to be strictly additive on $^3J_{\text{HH}}$. $\Delta\chi_{i(\text{g})}$ represents the group electronegativity in the Huggins scale of the substituent *i*. This formalism includes

the electron-withdrawing or donating effect of the β -substituents attached to α substituents. ζ_i ($= \pm 1$) accounts for the orientation of the substituent *i* on the H–C–C–H fragment with respect to the coupling protons. The set of P_1 – P_7 parameters can be adjusted depending upon how many nonproton substituents the H–C–C–H fragment carries. We have herein used the values for P_1 – P_7 parameters obtained originally by Haasnoot–Altona^{17b} to perform PSEUROT analyses for **1–3**.

(ii) Translation of the $\Phi_{\text{H-C-C-H}}$ (Φ_{HH}) Torsion Angles into the Endocyclic Torsion Angles (Step 4a of Scheme 2). Each Φ_{HH} is subsequently used to calculate an endocyclic torsion [i.e., ν_0 (C4'–C6'–C1'–C2'), ν_1 (C6'–C1'–C2'–C3'), ν_2 (C1'–C2'–C3'–C4'), ν_3 (C2'–C3'–C4'–C6'), or ν_4 (C3'–C4'–C6'–C1')] using the linear relationship $\Phi_{\text{HH}} = A\nu_i + B$. In the case of pentofuranosyl nucleosides, *A* and *B* values have been derived¹⁴ from a large set of crystal structures available. In the case of carbocyclic nucleosides, there are only very few crystal structures^{7–10} known, so that for these compounds the reliability of the *A* and *B* parameters derived only on the basis of crystal structures remains questionable.

We have therefore obtained pairs of the *A*, *B* parameters for each H–C–C–H fragment in **1–3** from a set of 12 structures optimized by ab initio calculations at the HF/3-21G* level (section IIIB). All ab initio calculations have been performed by constraining only the geometry (*P* and Ψ_{m}) of the cyclopentane ring. The Φ_{HH} torsions vs the corresponding 5 endocyclic torsions (ν_0 – ν_4) for the ab initio optimized conformers are plotted in Figure 4. From the slopes and intercepts of the correlation plots of Φ_{HH} vs ν_i for **1–3** we have calculated the values of the *A* and *B* parameters for all (Φ_{HH} , ν) pairs (Table 2).

(iii) Translation of the Endocyclic Torsion Angles into the Pseudorotational Parameters (Step 5a in Scheme 2). The phase angle and puckering amplitude

(17) (a) De Leeuw, F. A. A. M.; Altona, C. *J. Comput. Chem.* **1983**, *4*, 428 and PSEUROT, QCPE program No 463. (b) Haasnoot, C. A. G.; de Leeuw, F. A. A. M.; Altona, C. *Tetrahedron* **1980**, *36*, 2783.

(18) Gaussian 94, Revision C.3: Frisch, M. J.; Trucks, G. W.; Schlegel, H. B.; Gill, P. M. W.; Johnson, B. G.; Robb, M. A.; Cheeseman, J. R.; Keith, T.; Petersson, G. A.; Montgomery, J. A.; Raghavachari, K.; Al-Laham, M. A.; Zakrzewski, V. G.; Ortiz, J. V.; Foresman, J. B.; Cioslowski, J.; Stefanov, B. B.; Nanayakkara, A.; Challacombe, M.; Peng, C. Y.; Ayala, P. Y.; Chen, W.; Wong, M. W.; Andres, J. L.; Replogle, E. S.; Gomperts, R.; Martin, R. L.; Fox, D. J.; Binkley, J. S.; Defrees, D. J.; Baker, J.; Stewart, J. P.; Head-Gordon, M.; Gonzalez, C.; Pople, J. A. Gaussian, Inc., Pittsburgh, PA, 1995.

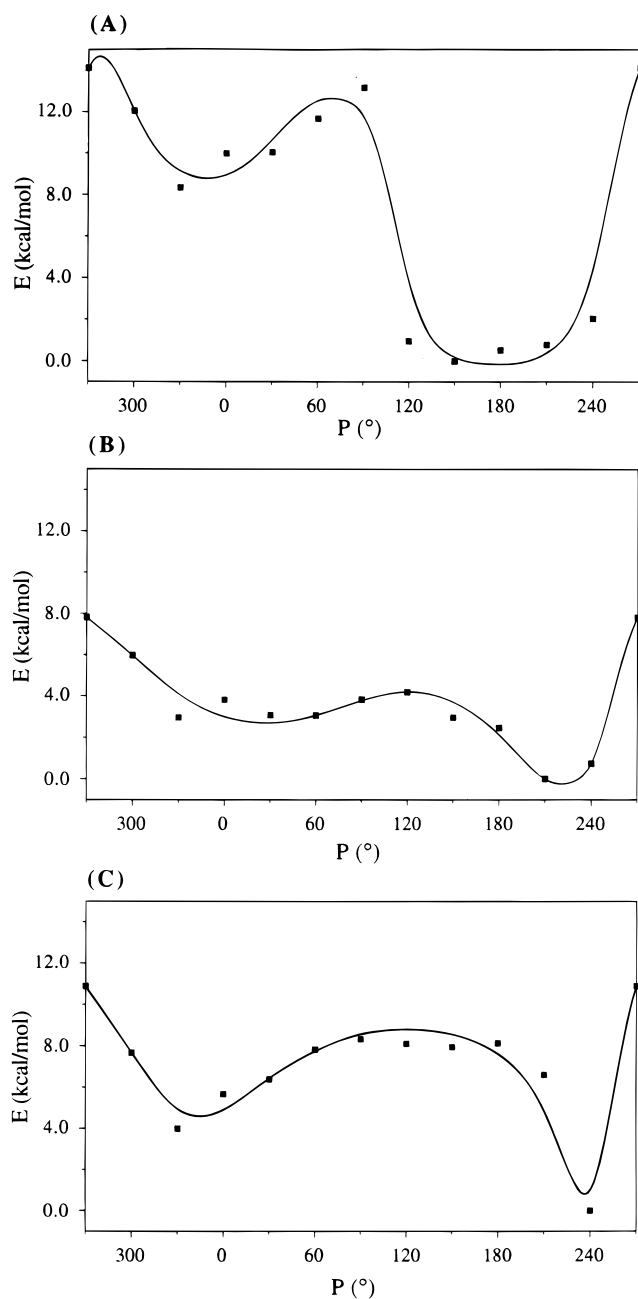


Figure 2. Plots of the energy (E) as a function of the phase angle of pseudorotation (P) for 12 ab initio optimized structures of **1–3** (see section IIIB in the text). The calculations have been performed at HF/3-21G* level using GAUSSIAN 94 program (ref 18) by constraining only two endocyclic torsions (ν_0 and ν_4) to the appropriate values in order to sweep P from 0 to 360° in 30° intervals at a common Ψ_m value (41°), whereas the rest of the molecule has been freely optimized. The same starting geometry around β (180°), γ (180°), χ (-120°), ϵ_2 [C1'-C2'-O2'-H] (180° in **1** and **3**) and ϵ_3 [C4'-C3'-O3'-H] (-60° for **1** and 180° for **2**) torsions has been used for all 36 optimizations. The preferred conformation for the lowest energy structures is χ anti, γ^t for **1–3**, $\epsilon_2 \sim 60^\circ$ for **1** and **3**, and ϵ_3 trans for **1** and **2**.

of the N-type [P_N and $\Psi_m(N)$] and S-type [P_S and $\Psi_m(S)$] conformers are derived from the pseudorotational law (eq 2)

$$\nu(j) = \Psi_m * \cos(P + 4\pi(j - 2)/5) \quad (2)$$

where $\nu(j)$ is an endocyclic torsion angle. For practical

purposes, eq 2 can be regarded as nearly exact for equilateral five-membered rings such as cyclopentane, as it is able to reproduce the cyclopentane torsions with an accuracy better than 0.1°. ¹⁹ We have, however, carefully checked the influence of the substituents attached to the cyclopentane ring in the case of aristeromycin (**1**) by comparing the values of endocyclic torsions calculated using eq 2 with those obtained using eq 3

$$\nu(j) = \Psi_m * a(j) * \cos(P + \epsilon(j) + 4\pi(j - 2)/5) \quad (3)$$

where $a(j)$ and $\epsilon(j)$ are correction factors that should overcome small differences in the C–C bond lengths in the cyclopentane ring of **1** because of different substituents at C1' and C4'.

In order to find out the $a(j)$ and $\epsilon(j)$ pairs for all endocyclic torsions $\nu(j)$, we have fully optimized²⁰ two conformers of aristeromycin using GAUSSIAN 94 at HF/6-31G* level using a dielectric constant of 78.3 D in SCRF. We have chosen to optimize the two energy minima found from the energy profile shown in Figure 2 for aristeromycin (**1**). The starting geometry for the first conformer of **1** was taken as $P = 150^\circ$ with $\Psi_m = 41^\circ$, whereas for the second pseudorotamer it was defined by $P = 330^\circ$ with $\Psi_m = 41^\circ$. After optimization by ab initio calculations, the two conformers have the following geometries: $P = 145^\circ$, $\Psi_m = 43^\circ$ and $P = 50^\circ$, $\Psi_m = 44^\circ$, respectively, and the former was preferred by 3.6 kcal/mol. To calculate $a(2)$ and $\epsilon(2)$, for instance, we have first substituted the values of $\nu(2)$, P , and Ψ_m of the first optimized structure of **1** into eq 3. By repeating this operation for the second optimized conformer of **1**, we generated a system of two equations with two unknowns, which could be solved easily.

For each endocyclic torsion $\nu(j)$, the calculated $a(j)$ and $\epsilon(j)$ values²¹ are very close to 1.0 and 0.0, respectively,

(19) Haasnoot, C. A. G.; De Leeuw, F. A. A. M.; De Leeuw, H. P. M.; Altona, C. *Biopolymers* **1981**, *20*, 1211.

(20) The ab initio calculations at HF/6-31G* using a dielectric constant of 78.3 D in SCRF mode were started from the two lowest energy minima found in the energy plots (Figure 2) for **1–3**. For **2**, the free optimization of the initial (HF/3-21G* optimized) two conformers ($P = 330^\circ$ and $\Psi_m = 41^\circ$) and ($P = 210^\circ$ and $\Psi_m = 41^\circ$) resulted in a very similar S-type geometry: ($P = 140^\circ$ and $\Psi_m = 44^\circ$) and ($P = 137^\circ$ and $\Psi_m = 44^\circ$), respectively, with the former being preferred by ~1 kcal/mol. For **3**, the free optimization of the initial (HF/3-21G* optimized) conformers ($P = 240^\circ$ and $\Psi_m = 41^\circ$) and ($P = 330^\circ$ and $\Psi_m = 41^\circ$) resulted in ($P = 222^\circ$ and $\Psi_m = 40^\circ$) and ($P = 127^\circ$ and $\Psi_m = 44^\circ$), respectively, with the former stabilized by ~1 kcal/mol. The convergence of the two low-energy N-type and SW-type states of **2** from HF/3-21G* to HF/6-31G* to a very similar S-type geometry goes hand in hand with the experimental plot of $^3J_{3'4'}$ versus $^3J_{1'2'}$ for **2**, since as the temperature is increased from 278 to 358 K, the population of the major conformers is hardly reduced. This is, however, in contrast with the PSEUROT calculations on the basis of the assumption of the two-state equilibrium, which shows that the population of the minor N-type conformation is about 20% at all temperatures [sections (III), D, ii and (VI), C]. We have, however, performed a second set of PSEUROT calculations (either with Haasnoot–Altona's or our reparametrized Karplus equation) considering a single state for **2**: We have scanned P and Ψ_m and values in the ranges $90^\circ < P < 120^\circ$ (in 10° steps) with $35^\circ < \Psi_m < 45^\circ$ (in 2° steps), consistent with our qualitative observation of the predominant conformational state of **2** in the plot shown in Figure 4C. All analyses of these grid searches on the basis of the above conformational hyperspace converged to $P = 103.5^\circ$ with $\Psi_m = 31.5^\circ$ (in the case of Altona's equation, rms error = 0.9 Hz with ΔJ_{\max} error = 1.9 Hz) and to $P = 105.3^\circ$ with $\Psi_m = 31.6^\circ$ (in the case of our reparametrized Karplus (eq 4), rms error = 1.1 Hz with ΔJ_{\max} error = 2.1 Hz). Thus, the comparison of the rms and ΔJ_{\max} errors resulting from the PSEUROT analyses based upon a two-state model (Table 3) versus one state clearly shows the prevalence of the former.

(21) The $a(j)$ and $\epsilon(j)$ values are as follows: $a(0) = 0.996$ and $\epsilon(0) = 0.043$; $a(1) = 0.998$ and $\epsilon(1) = 0.265$; $a(2) = 1.000$ and $\epsilon(2) = -0.052$; $a(3) = 1.005$ and $\epsilon(3) = 0.059$; $a(4) = 0.994$ and $\epsilon(4) = -0.1334$.

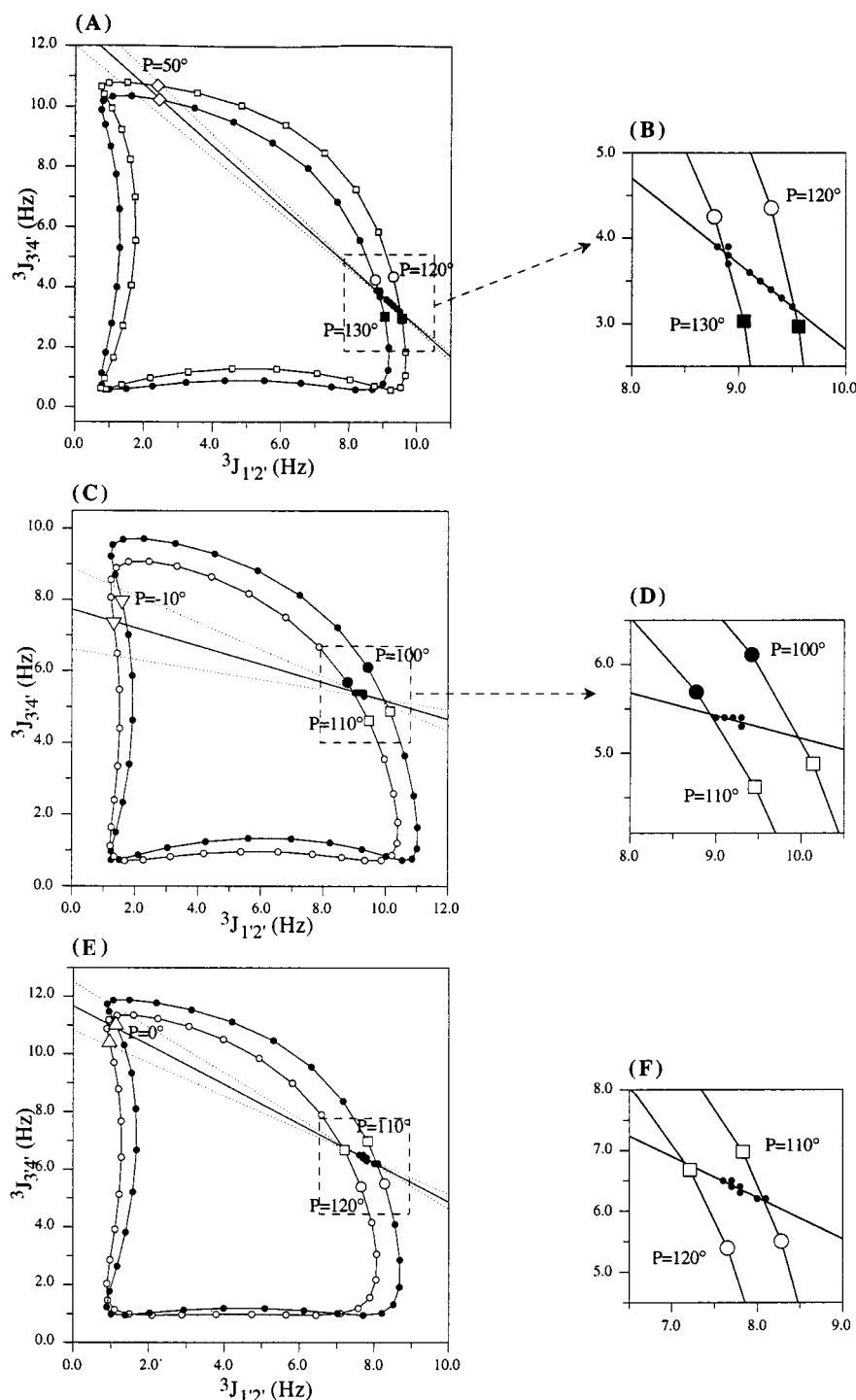


Figure 3. Plots of the calculated variation of ${}^3J_{3'4'}$ vs ${}^3J_{1'2'}$ at 36 phase angle values (from 0° to 350° in 10° steps) and two puckering amplitudes for **1** [40° (\bullet) and 45° (\square)], **2** and **3** [35° (\circ) and 40° (\bullet)]. The dependence of ${}^3J_{1'2'}$ and ${}^3J_{3'4'}$ on P and Ψ_m for **1–3** has been calculated using the PSEUROT program (steps 3a–5a in Scheme 2 and ref 17). Through the experimental data points of temperature-dependent (278–358 K, 10 K intervals, Table 1) ${}^3J_{3'4'}$ vs ${}^3J_{1'2'}$ shown by \bullet in all panels, we have fitted three straight lines: (i) The “best” straight line (shown by $-$). (ii) Two additional straight lines (marked by \cdots) in such a way that their slopes and intercepts differ by $\pm\sigma$ (i.e., the standard deviation) from the slopes and intercepts of the best fitted lines in order to estimate the range of phase angle values accessible to the minor N-type pseudorotamer in the two-state equilibria of **1–3** (see the text, section III). The experimental points and their vicinity (surrounded by a dashed square) can better be seen as focused in panels B, D, and F for **1–3**, respectively. (A) Variation of ${}^3J_{3'4'}$ vs ${}^3J_{1'2'}$ for aristeromycin (**1**). The slope and intercept of the best fitted line through the experimental data of ${}^3J_{3'4'}$ vs ${}^3J_{1'2'}$ are -1.0 ($\sigma = 0.1$) and 12.7 ($\sigma = 0.7$). According to the extrapolation of the fitted lines and the location of the experimental points, the phase angles of the minor N-type and major S-type pseudorotamers of **1** have been found in the following ranges: $\sim 35^\circ < P_{N\text{-type}} < \sim 60^\circ$ and $\sim 120^\circ < P_{S\text{-type}} < \sim 130^\circ$ respectively. (C) Variation of ${}^3J_{3'4'}$ vs ${}^3J_{1'2'}$ for 2'-deoxyaristeromycin (**2**). The slope and intercept of the best fitted line through the experimental data of ${}^3J_{3'4'}$ vs ${}^3J_{1'2'}$ are -0.3 ($\sigma = 0.1$) and 7.7 ($\sigma = 1.1$). The phase angles of the minor N-type and major S-type pseudorotamers of **2** have been found in the following ranges: $\sim -20^\circ < P_{N\text{-type}} < \sim 10^\circ$ and $\sim 100^\circ < P_{S\text{-type}} < \sim 110^\circ$, respectively. (E) Variations of ${}^3J_{3'4'}$ vs ${}^3J_{1'2'}$ for 3'-deoxyaristeromycin (**3**). The slope and intercept of the best fitted line through the experimental data of ${}^3J_{3'4'}$ vs ${}^3J_{1'2'}$ have been calculated as -0.7 ($\sigma = 0.1$) and 11.7 ($\sigma = 0.8$). Qualitative analyses of the phase angles of the minor N-type and major S-type pseudorotamers of **3** have resulted in the following ranges: $\sim 0^\circ < P_{N\text{-type}} < \sim 30^\circ$ and $\sim 110^\circ < P_{S\text{-type}} < \sim 120^\circ$, respectively.

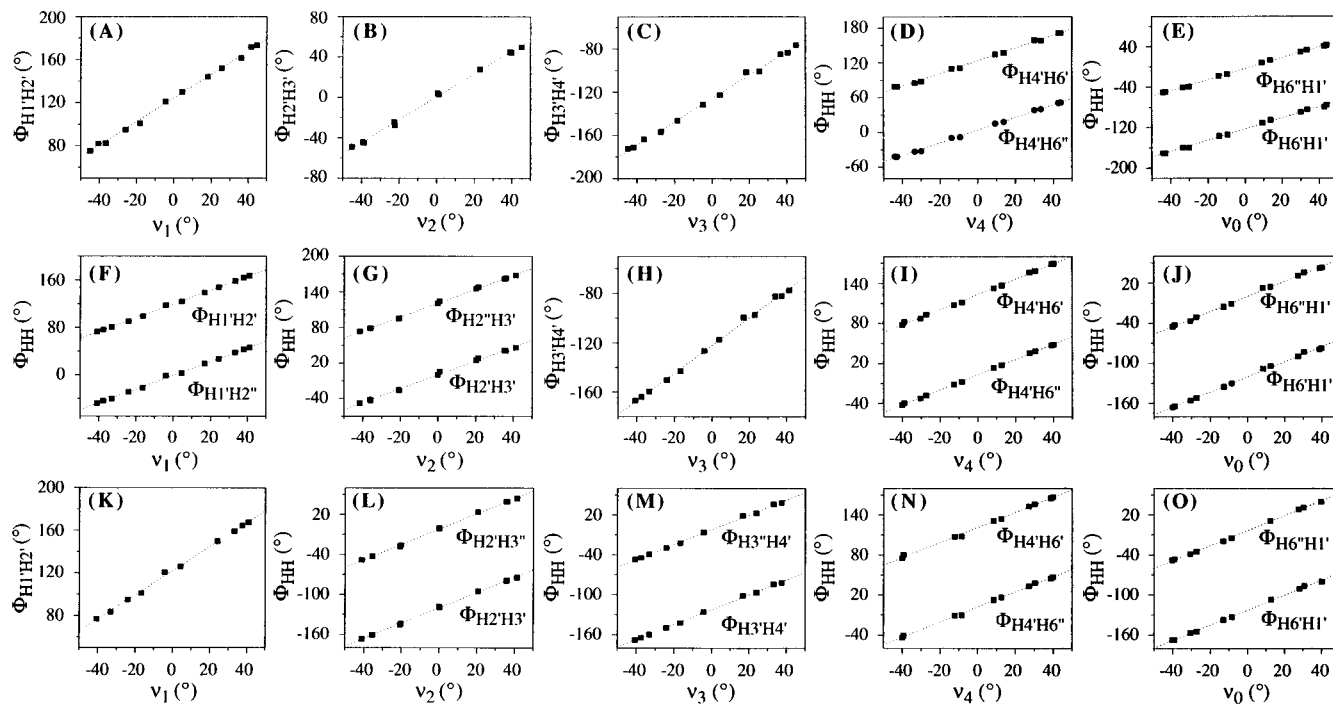


Figure 4. Correlation plots of proton–proton torsion angles (Φ_{HH}) as a function of endocyclic torsion angles (ν_i where $i = 0-4$) for **1–3**. For each compound, Φ_{HH} and ν_i torsions have been extracted from 12 ab initio optimized structures ($P = 0-330^\circ$ in 30° steps with $\Psi_m = 41^\circ$ for all structures, see Section IIIB for the details of the calculations). Each of the straight lines fitted with Profit program (ref 39) through the 12 (Φ_{HH} vs ν_i) pairs in the plots shown in panels A–O has a correlation coefficient >0.95 . The slopes and intercepts of these straight lines have given the pairs of (A , B) parameters (and their standard deviations), respectively Panels F–J: correlation plots of proton–proton torsions vs endocyclic torsions for 2'-deoxyaristeromycin (**2**). Panels K–O: correlation plots of proton–proton torsions vs endocyclic torsions for 3'-deoxyaristeromycin (**3**).

which clearly shows that the effect of the nucleobase, 2'-OH, 3'-OH, and of 4'-CH₂OH on the endocyclic C–C bond lengths of **1** is negligible. Therefore, the geometry of aristeromycin pseudorotamers can accurately be treated by eq 2.

(D) Results of the Pseudorotational Analyses of 1–3 (Steps 3a–5a) in Scheme 2 and Table 3]. (i) Qualitative Pseudorotational Analyses of $^3J_{\text{HH}}$ Couplings in 1–3 Using Plots of the Calculated Variation of $^3J_{3'4'}$ vs $^3J_{1'2'}$ for Different Constrained Values of P and Ψ_m [Steps (3a) – (5a) in Scheme 2]. Using PSEUROT, we have first calculated the dependence of $^3J_{1'2'}$ and $^3J_{3'4'}$ on the phase angle (P) at two Ψ_m values for aristeromycin [40° and 45°], 2'-deoxyaristeromycin, and 3'-deoxyaristeromycin [35° and 40°]. The plots of $^3J_{3'4'}$ versus $^3J_{1'2'}$ for **1–3** have subsequently been constructed (Figure 3). These plots show that the conformation of the cyclopentane ring in **1–3** is strongly biased ($\geq 90\%$) toward ${}^1\text{E}$ - or ${}^0\text{T}$ -type forms (i.e., $P \sim 125^\circ$ for **1**, $\sim 105^\circ$ for **2**, and $\sim 115^\circ$ for **3**), as evident by the accumulation of the experimental data points in these regions. As the temperature is increased from 278 to 358 K, the population of these major conformers is only slightly reduced. Nevertheless, it is possible to fit a

straight line through the temperature-dependent experimental data. This suggests that the cyclopentane ring in **1–3** is involved in a conformational equilibrium between two species, a major [${}^1\text{E}$ – ${}^0\text{T}$]-type conformer and a minor pseudorotamer, the geometry of which cannot be defined unambiguously. In order to estimate the geometry of the minor species in a two-state conformational equilibria of **1–3**, we have used the following procedure: (i) The slopes and intercepts of the best straight lines fitted through our temperature-dependent experimental ($^3J_{3'4'}$, $^3J_{1'2'}$) pairs for **1–3** are associated with certain standard deviations (σ) (see the legend of Figure 4). (ii) In the plots shown in Figure 4, we have also drawn two additional straight lines in such a way that their slopes and intercepts differ by $\pm\sigma$ from the slopes and intercepts of the best fitted lines. (iii) The acceptable phase angle values for the N-type conformers of **1–3** have been taken within the limits defined by the two outer straight lines drawn in panels A, C, and E of Figure 4, i.e., $35^\circ < P_{\text{N-type}} < 60^\circ$ with $\Psi_m = 42 \pm 3^\circ$ for **1**, $340^\circ < P_{\text{N-type}} < 10^\circ$ with $\Psi_m = 38 \pm 3^\circ$ for **2**, and $0^\circ < P_{\text{N-type}} < 30^\circ$ with $\Psi_m = 38 \pm 3^\circ$ for **3**.

(ii) Hyperspace of Conformations That Is Accessible to the Cyclopentane Rings in 1 and 3 (Steps 3a–5a in Scheme 2). Using the program PSEUROT¹⁷ (version 3B) in which the Haasnoot–Altona Karplus equation is implemented with the original set of P_1 – P_7 parameters,^{17b} we have analyzed the sets of temperature-dependent $^3J_{\text{HH}}$ (Table 1) for **1–3** in terms of two-state N-type \rightleftharpoons S-type equilibria.

The plots of $^3J_{3'4'}$ versus $^3J_{1'2'}$ imply that the conformational equilibria of cyclopentane in **1–3** are strongly

(22) We have calculated the theoretical vicinal $^3J_{\text{HH}}$ for aristeromycin, assuming that its cyclopentane ring has the same conformation as that found in its X-ray crystal structure. From the crystal structure of **1**, we have extracted the endocyclic torsion angles ($\nu_0 - \nu_4$). Using the A and B parameter sets developed on the basis of ab initio optimized structures (section (III), C, (ii)), we have derived a proton-substituted Haasnoot–Altona's Karplus-type equation (eq 1, ref 17b) to obtain the corresponding $^3J_{\text{HH}}$ values. The results are as follows: $^3J_{1'2'} = 6.8$ Hz, $^3J_{2'3'} = 7.4$ Hz, $^3J_{3'4'} = 8.3$ Hz, $^3J_{4'6'} = 11.9$ Hz, $^3J_{4'6''} = 5.4$ Hz, $^3J_{6'1'} = 10.9$ Hz, $^3J_{6'1''} = 6.0$ Hz.

Table 3. PSEUROT^a Analyses Results Obtained by Using the Original Haasnoot–Altona Karplus Equation and Our Reparametrized Karplus Equation

compd	pseurot analyses performed using Haasnoot–Altona's Karplus equation ^b						pseurot analyses performed using our reparametrized equation ^c					
	minor conformers' geometries				lowest rms value	lowest ΔJ_{\max}	minor conformers' geometries				lowest rms value	lowest ΔJ_{\max}
	P_{\min}	Ψ_m^{\min}	P_{\max}	Ψ_m^{\max}			P_{\min}	Ψ_m^{\min}	P_{\max}	Ψ_m^{\max}		
aristeromycin (1)	35–65	35	128–130	34–35	0.64	1.3	35–65	35	134–137	37–38	0.53	1.0
	35–65	37	129–130	35–36	0.64	1.4	35–65	37	134–138	37–38	0.52	1.0
	35–65	39	129–131	35–36	0.64	1.4	35–65	39	134–139	37–38	0.52	1.0
	35–65	41	129–131	35–36	0.64	1.4	35–65	41	134–139	37–38	0.51	1.0
	35–65	43	129–131	35–36	0.64	1.4	35–65	43	134–139	37–38	0.51	0.9
	35–65	45	129–131	35–36	0.64	1.4	35–65	45	135–140	37–38	0.50	1.0
2'-deoxyaristeromycin (2)	–30–10	35	106–112	34–36	0.61	1.0	–30–10	35	108–116	38–39	0.52	0.8
	–30–10	37	106–112	34–36	0.60	1.0	–30–10	37	108–116	37–39	0.51	0.8
	–30–10	39	105–112	34–36	0.59	1.0	–30–10	39	108–116	37–38	0.50	0.8
	–30–10	41	105–112	34–36	0.58	1.0	–30–10	41	108–116	37–38	0.50	0.8
	–30–10	43	105–112	34–36	0.57	1.0	–30–10	43	108–116	36–37	0.49	0.8
	–30–10	45	105–112	34–36	0.56	1.0	–30–10	45	107–116	36–37	0.49	0.8
3'-deoxyaristeromycin (3)	–20–40	35	118–123	35–38	0.67	1.5	–20–40	35	120–127	37–40	0.62	1.3
	–20–40	37	118–123	35–38	0.66	1.6	–20–40	37	120–127	37–40	0.61	1.3
	–20–40	39	118–123	35–38	0.66	1.6	–20–40	39	120–127	37–39	0.59	1.3
	–20–40	41	118–123	35–38	0.65	1.6	–20–40	41	120–127	37–39	0.58	1.3
	–20–40	43	118–123	35–38	0.65	1.5	–20–40	43	119–127	37–39	0.57	1.3
	–20–40	45	118–123	35–38	0.64	1.5	–20–40	45	119–127	37–38	0.56	1.3

^a Version 3B of the program PSEUROT (ref 17) has been used to perform all calculations (see Scheme 2 for the steps involved in the PSEUROT algorithm). The quality of an iteration with PSEUROT is reflected in the values of the rms (Hz) and ΔJ_{\max} (Hz) errors, which represent the root mean squares error and the largest difference between the experimental coupling constants and those back-calculated by the program, respectively. All phase angles and puckering amplitudes are given in degrees. ^b We have initially used the original Haasnoot–Altona Karplus equation implemented in PSEUROT 3B (eq 1) where P_1 – P_7 coefficients are determined by the substitution patterns of H–C–C–H fragments (ref 17b and Section III). ^c These sets of analyses are based upon our reparametrized Karplus-type equation (eq 4) and section VIB). ^d P_{\min} of the minor N-type pseudorotamer has been constrained in the range from 35° to 65° for **1**, from –30° to 10° for **2**, and from –20° to 40° for **3** in 15° intervals. For each value of P_{\min} , the corresponding puckering amplitude of the minor conformer (Ψ_m^{\min}) has been constrained in the range from 35° to 45° in 2° resolution.

biased toward ${}_1E$ or ${}_1T$ forms; therefore, we have performed all PSEUROT calculations by constraining P and Ψ_m of the minor “N-type” conformer in the ranges given previously [section IIID (i)]. The multilinear fitting procedure of PSEUROT showed that the experimental temperature-dependent ${}^3J_{\text{HH}}$ for **1–3** are better reproduced when their constituent cyclopentane rings are involved in the following equilibria (Tables 3 and 4): (35° < P [${}^3T - {}^0T$] < 65°, 35° < Ψ_m < 45°) \rightleftharpoons (128° < P [${}_1E$] < 131°, 34° < Ψ_m < 36°) for **1**, (330° < P [${}^1T - {}^3E$] < 10°, 35° < Ψ_m < 45°) \rightleftharpoons (105° < P [${}_1T$] < 112°, 34° < Ψ_m < 36°) for **2** and (340° < P [${}_2E - {}^3T$] < 40°, 35° < Ψ_m < 45°) \rightleftharpoons (118° < P [${}_1E$] < 123°, 35° < Ψ_m < 38°) for **3**. The population of the major conformers [${}_1T$ or ${}_1E$ -type] of **1–3** was found to be >90% for **1**, >80% for **2**, and >85% for **3** at 278 K.

The lowest ΔJ_{\max} and rms errors from the best PSEUROT analyses of **1–3** (rms ca. 0.6–0.7 Hz for **1–3**, $\Delta J_{\max} = 1.3$ Hz for **1**, 1.0 Hz for **2**, and 1.5 Hz for **3**) are still rather large in the view of the accuracy of other pseudorotational analyses previously performed on β -D-2',3'-dideoxynucleosides, where 8 vicinal proton–proton coupling constants are available to assess the sugar conformation^{3c} ($\Delta J_{\max} = 0.8$ –1.0 Hz and rms = 0.4–0.6 Hz for 2',3'-dideoxyadenosine).

This suggests that the geometries of the cyclopentane rings in **1–3** are not accurately defined by the PSEUROT calculations. Furthermore, since the above solution structure of aristeromycin **1** is very different from its X-ray structure (see above), the question remains whether the solution structure derived by the original parametrization^{17b} of the Karplus-type equation implemented

in PSEUROT is adequate for defining the solution conformation of carbocyclic nucleosides (vide infra, section V and VI). It was clear that this required verification by an independent Karplus equation before questioning the validity of the solid state structure in the solution.

(IV) The Comparison (Step 8 in Scheme 2) of the X-ray Crystal Structure of Aristeromycin (Steps 6 and 7 in Scheme 2) with the NMR-PSEUROT Analyses Results (Steps 3a–5a). As stated above, the X-ray crystal structure of aristeromycin (**1**) and its NMR-PSEUROT-derived geometry are different (Tables 3 and 4). In the solid state, the cyclopentane ring in **1** adopts an East-type conformation (0E , see above), whereas our pseudorotational analyses show a predominance for [${}_1T$ or ${}_1E$ -type]-type forms (section IIID). The difference between crystal and aqueous solution structures of **1** has been *quantified* by calculating the theoretical ${}^3J_{\text{HH}}$ and comparing them with the experimental ${}^3J_{\text{HH}}$ for aristeromycin ($\Delta J_{\max} = 4.7$ Hz, ref 22). This ΔJ_{\max} difference confirms that aristeromycin (**1**) takes up different conformations in the solid state and in aqueous solution, as has been found in the case of some pentofuranosyl nucleosides. For instance, it has been shown that adenosine²³ crystallizes as the North-type conformer ($P = 7^\circ$, $\Psi_m = 37^\circ$), whereas its hydrochloride salt crystallizes as the S-type form.²⁴ Furthermore, NMR studies suggest a clear preference (~67% at room temperature) for the S-type pseudorotamers at neutral pD, and the equilibrium is shifted further to the North at acidic pD (~55%

(23) Lai, T. F.; Marsh, R. E. *Acta Crystallogr.* **1972**, B28, 1982.(24) Shikata, K.; Ueki, T.; Mitsui, T. *Acta Crystallogr.* **1973**, B29, 31.

Table 4. Comparative Conformations^a of Aristeromycin (1), 2'-deoxyaristeromycin (2), and 3'-deoxyaristeromycin (3) As Obtained from Crystal Structure^b and NMR-PSEUROT^c Analyses

compd	geometries	X-ray ^b structure	NMR-PSEUROT analyses	
			using Altona's Karplus equation ^c	using our reparametrized Karplus equation ^c
aristeromycin (1)	ν_0	-37.5	-32.6	-33.0
	ν_1	23.5	34.0	37.0
	ν_2	1.0	-22.4	-26.9
	ν_3	-25.7	2.3	6.6
	ν_4	39.3	18.8	16.3
	P	89.0	129.7	136.1
	Ψ_m	40.8	35.1	37.4
	χ	-113.5	<i>d</i>	<i>d</i>
	γ	-137.9	<i>e</i>	<i>e</i>
2'-deoxyaristeromycin (2)	ν_0		-35.5	-37.3
	ν_1		29.4	31.6
	ν_2		-12.1	-13.9
	ν_3		-9.8	-9.2
	ν_4		28.0	28.7
	P		109.9	111.8
	Ψ_m		35.5	37.4
	χ		<i>d</i>	<i>d</i>
	γ		<i>e</i>	<i>e</i>
3'-deoxyaristeromycin (3)	ν_0		-36.0	-36.8
	ν_1		33.9	35.6
	ν_2		-18.8	-20.9
	ν_3		-3.5	-1.9
	ν_4		24.4	23.9
	P		120.6	123.2
	Ψ_m		36.9	38.1
	χ		<i>f</i>	<i>f</i>
	γ		<i>e</i>	<i>e</i>

^a All torsions, P , and Ψ_m are given in degrees. $\nu_0, \nu_1, \nu_2, \nu_3$, and ν_4 in column 2 represent the endocyclic torsion angles for the carbocyclic moieties, and they have been used to derive the phase angle of pseudorotation (P) and maximum puckering amplitude (Ψ_m) (see ref 13). χ is the glycosyl torsion angle, which is defined as $[\text{C}_4\text{-N}_9\text{-C}_1\text{-C}_6]$. ^b The coordinates used to build the X-ray crystal structure of aristeromycin (1) have been taken from ref 7. No X-ray crystal structure is available for 2'-deoxy- and 3'-deoxyaristeromycin. ^c $\nu_0, \nu_1, \nu_2, \nu_3$, and ν_4 in columns 4 and 5 have been calculated from the average P and Ψ_m values of the major pseudorotamer for 1–3 using the best results of the PSEUROT calculations. The PSEUROT calculations have been performed using either (i) Altona et al.'s set of parameters in the Karplus-type equation (eq 1) that is implemented in the program (i.e., column 4) or (ii) our set of new parameters in the Karplus-type equation (eq 4) (i.e., column 5) (see Table 3 for the hyperspace of the geometries covered during the calculations). ^d The relative populations of syn vs anti conformers around glycosyl torsion have been calculated from NOE enhancements, using the method developed by Rosemeyer et al. (ref 42): 56 ± 7% anti-aristeromycin and 54 ± 14% anti-2'-deoxyaristeromycin. ^e The populations of the three γ rotamers [γ^+ , γ^- , and γ^t] around the $[\text{O}_5\text{-C}_5\text{-C}_4\text{-C}_3]$ torsion have been determined from $^3J_{4'5'}$ and $^3J_{4'5''}$ (ref 40), taking the electronegativity of the substituents in carbocyclic nucleosides into consideration (see ref 41): 22% γ^+ , 37% γ^- , and 41% γ^t for aristeromycin; 26% γ^+ , 31% γ^- , and 43% γ^t for 2'-deoxyaristeromycin, and 18% γ^+ , 38% γ^- , and 44% γ^t for 3'-deoxyaristeromycin. ^f Rosemeyer's method (ref 42 and footnote d), which has been applied in order to establish the conformation around the glycosyl torsion in 1 and 2, could not be used for 3'-deoxyaristeromycin because $\text{H}_{1'}$ and $\text{H}_{2'}$ are almost isochronous, and this remains true at any pD value in the acidic or neutral ranges.

South conformer at 298 K).³ⁿ Similarly, it is known that 3'-azidothymidine²⁵ in D_2O is involved in an equipopulated two-state $\text{N} \rightleftharpoons \text{S}$ equilibrium, despite the fact that it crystallizes in the S-type puckered forms ($P = 175^\circ$, $\Psi_m = 32^\circ$).²⁶ 3'-Fluorothymidine, on the other hand, crystallizes²⁷ as the South-type conformers, but the P value of this structure (average $P = 171^\circ$, $\Psi_m = 34^\circ$) deviates from the P value ($P \sim 160^\circ$, $\Psi_m = 34^\circ$) found for

the preferred ($\geq 90\%$) S-type sugar geometry by ^1H NMR studies.²⁵ For all $\beta\text{-D-}2',3'\text{-dideoxynucleosides}$ (ddNs), the pentofuranose sugar is mostly puckered as the N-type conformer in D_2O solution^{3c} ($\geq 75\%$ at 298K), whereas in the solid state²⁸ it adopts the S-type geometry ($P = 194^\circ$, $\Psi_m = 37^\circ$ for ddA, $P = 208^\circ$ and $\Psi_m = 34^\circ$ for ddC). In the case of aristeromycin (1), the question remains whether the discrepancy found between the NMR-PSEUROT structure and X-ray crystal structure is a result of deficiency of the NMR-PSEUROT method or whether it is an intrinsic conformational property of aristeromycin in solid vis-à-vis solution state.

(V) The Revision of the PSEUROT Methodology by Modification of the Karplus Equation. The Haasnoot–Altona Karplus-type equation is based in particular on conformationally rigid substituted six membered rings. Due to the choice of conformationally rigid structures, the torsion angles were clustered mainly in the gauche and trans regions. This parametrization^{17b} also involves correlation of $^3J_{\text{HH}}$ with the corresponding torsion angles obtained from structures optimized with MM1 force field parameters.

This has led us to investigate whether the use of a Karplus-type equation parametrized with a dataset based exclusively on crystal structures of conformationally constrained nucleosides would improve the approach.

(VI) Reparametrization of the Seven-Term Haasnoot–Altona Karplus Equation (Steps 9 and 10 in Scheme 2). (A) Construction of a Data Set of Experimental $^3J_{\text{HH}}$ vs Φ_{HH} Torsion Angles for the Reparametrization (Step 9). Our dataset for the reparametrization of the Karplus equation is solely composed of constrained nucleosides, either natural or modified, that have been carefully selected based on the torsion angles and corresponding coupling constants encompassing the entire range of cisoid, transoid, and gauche regions, in fact, the entire 0–360° range. In this regard, we have particularly included eight torsions in the cis range from 330° to 30° and six torsions from 80° to 100°. The former group of data defines the second maximum position of the Karplus plots, whereas the latter range defines precisely the value of the coupling constant at the absolute minimum. The following considerations are taken into account for the choice of compounds in our dataset (Table 5 for the experimental $^3J_{\text{HH}}$ as a function of the solid state Φ_{HH} torsion angle for each compound).

(a) The flexibility of the ribose moiety in 3',5'-cyclic nucleotides²⁹ is considerably reduced in comparison with that of the pentofuranose sugar in the parent 3'- or 5'-

(25) Plavec, J.; Koole, L. H.; Sandström, A.; Chattopadhyaya, C. *Tetrahedron* **1991**, *47*, 7363.

(26) (a) Birnbaum, G. I.; Giziewicz, J.; Gabe, E. J.; Lin, T. S.; Prusoff, W. H. *Can. J. Chem.* **1987**, *65*, 2135. (b) Camerman, A.; Mastropalo, D.; Camerman, N. *Proc. Natl. Acad. Sci. U.S.A.* **1987**, *84*, 8239. (c) van Roey, P.; Salerno, J. N.; Duax, W. L.; Chu, C. K.; Ahn, M. K.; Schinazi, R. F. *J. Am. Chem. Soc.* **1988**, *110*, 2277. (d) Parthasarathy, R.; Kim, H. *Biochem. Biophys. Res. Commun.* **1988**, *152*, 351. (e) Dyer, I.; Low, J. N.; Tollin, P.; Wilson, R.H.; Howie, R. W. *Acta Crystallogr.* **1988**, *C44*, 767. (f) Gurskaya, G. V.; Tsapkina, E. N.; Skaptasova, N. V.; Lindeman, A. A.; Struchkov, Yu. T. *Dokl. Akad. Nauk. USSR* **1986**, *291*, 854.

(27) (a) van Roey, P.; Schinazi, R. F. *Antiviral Chem. Chemother.* **1990**, *1*, 93. (b) Camerman, N.; Mastropalo, D.; Camerman, A. *Proc. Natl. Acad. Sci. U.S.A.* **1990**, *87*, 3534.

(28) (a) Chu, C. K.; Badhti, V. S.; Doboszewski, B.; Gu, Z. P.; Kosugi, Y.; Pullaiyah, K. C.; van Roey, P. *J. Org. Chem.* **1989**, *54*, 2217. (b) Birnbaum, G. I.; Lin, T. S.; Prusoff, W. H. *Biochem. Biophys. Res. Commun.* **1988**, *151*, 608.

(29) Lee, C.-H.; Sarma, R. H. *J. Am. Chem. Soc.* **1976**, *98*, 3541.

Table 5. Comparison of Experimental ${}^3J_{\text{HH}}^a$ with ${}^3J_{\text{HH}}^c$ Calculated by Our Reparametrized Seven-Term Karplus Equation (Eq 4) for 12 Conformationally Constrained Natural and Carbocyclic Nucleosides

no.	compd	input experimental data		results from reparametrization	
		Φ_{HH}^b	${}^3J_{\text{HH}}(\text{exp})^a$	${}^3J_{\text{HH}}(\text{calc})^c$	${}^3J_{\text{exp}} - {}^3J_{\text{calc}}$
1	(4) $J_{1'2'}$	88.6	0.7	0.5	0.2
2	(4) $J_{2'3'}$	39.2	5.6	4.7	0.9
3	(4) $J_{3'4'}$	189.4	9.8	9.6	0.2
4	(4) $J_{4'5'}$	184.5	10.7	10.7	0.0
5	(5) $J_{1'2'}$	104.7	0.7	1.0	-0.3
6	(5) $J_{2'3'}$	40.0	5.2	4.6	0.6
7	(5) $J_{3'4'}$	180.6	9.8	9.8	0.0
8	(5) $J_{4'5'}$	176.0	10.7	10.7	0.0
9	(6) $J_{1'2'}$	111.1	0.7	1.5	-0.8
10	(6) $J_{2'3'}$	35.3	5.3	5.2	0.1
11	(6) $J_{3'4'}$	181.6	10.2	9.8	0.4
12	(6) $J_{4'5'}$	181.2	10.7	10.8	-0.1
13	(7) $J_{2'3'}$	337.7	7.3	7.6	-0.3
14	(7) $J_{2''3'}$	99.8	1.4	1.2	0.2
15	(7) $J_{3'4'}$	259.6	1.2	1.2	0.0
16	(8) $J_{1'2'}$	88.7	0.5	1.4	-0.9
17	(8) $J_{1'2''}$	331.1	7.4	7.5	-0.1
18	(8) $J_{2'3'}$	29.4	8.2	8.7	-0.5
19	(8) $J_{2''3'}$	147.7	8.9	8.1	0.8
20	(9) $J_{1'2'}$	107.3	1.3	1.1	0.2
21	(9) $J_{2'3'}$	24.3	6.5	6.6	-0.1
22	(9) $J_{3'4'}$	216.4	8.9	8.6	0.3
23	(9) $J_{3'\text{Hc}}$	319.5	6.4	6.2	0.2
24	(9) J_{HaHc}	37.3	7.6	7.8	-0.2
25	(9) J_{HbHc}	152.7	10.8	10.9	-0.1
26	(10) $J_{1'2'}$	122.7	2.7	2.8	-0.1
27	(10) $J_{2'3'}$	338.8	6.4	6.7	-0.3
28	(11) $J_{1'2'}$	125.2	3.5	3.1	0.4
29	(11) $J_{2'3'}$	336.7	6.2	6.5	-0.3
30	(11) $J_{3'4'}$	244.0	2.7	2.6	0.1
31	(12) $J_{1'2'}$	133.9	3.1	4.4	-1.3
32	(12) $J_{2'3'}$	333.9	6.3	6.2	0.1
33	(13) $J_{1'2'}$	11.0	5.9	6.3	-0.4
34	(13) $J_{2'3'}$	90.2	0.6	0.6	0.0
35	(13) $J_{3'4'}$	263.1	1.6	0.8	0.8
36	(14) $J_{1'2'}$	93.0	0.3	0.5	-0.2
37	(14) $J_{2'3'}$	42.7	4.4	4.3	0.1
38	(14) $J_{3'4'}$	193.1	8.9	9.4	-0.5
39	(15) $J_{1'2'}$	172.0	11.7	11.9	-0.2
40	(15) $J_{1'2''}$	47.8	6.2	5.9	0.3
41	(15) $J_{2'3'}$	314.5	4.0	3.9	0.1
42	(15) $J_{2''3'}$	80.0	1.3	1.5	-0.2
43	(15) $J_{3'4'}$	252.1	1.4	1.6	-0.2
44	(15) $J_{4'6'}$	136.4	7.5	7.3	0.2
45	(15) $J_{1'6'}$	195.7	10.5	10.6	-0.1

^a ${}^3J_{\text{HH}}$ (Hz) have been extracted from 1D ${}^1\text{H}$ NMR spectra (see the experimental section for **7**, **8**, and **10–13**) or they have been taken from the literature (refs 29 for **4–6**, 32 for **9**, 38 for **14**, and 5 for **15**). ^b All torsions are in (deg) and have been taken from crystal structures (refs 30a–c for **4–6**, 31 for **7**, 6 for **8**, 32 for **9**, 33 for **10**, 34 for **11**, 35 for **12**, 36 for **13**, 37 for **14**, and 11 for **15**). Note that we have allowed a variation of $\pm 3^\circ$ in the values of all torsions from the crystal structure data because of deviations found between two crystal forms in two different unit cells. When H coordinates were absent in the crystal structures, we have added them assuming sp^3 geometry. We have also extracted proton–proton torsions using linear relationship (see section IIIC (ii)) and found deviations of maximum of $\pm 5^\circ$ from the proton–proton torsions derived based on the assumption of sp^3 geometry. ^c These ${}^3J_{\text{HH}}$ s have been calculated by our reparametrized Karplus equation (eq 4, section VIB) obtained via multilinear fit of experimental ${}^3J_{\text{HH}}$ (column 4) vs the crystal structure torsions (column 3).

monophosphate nucleotides. Due to the fact that the ribose ring and the 5'-exocyclic linkage are trans fused, the conformation of the constituent ribose moiety in 3',5'-cAMP (**4**), 3',5'-cGMP (**5**), and 3',5'-cUMP (**6**) is locked into a ${}^3\text{T}$ -type conformation both in solution (as determined from ${}^1\text{H}$ NMR spectroscopy) and in the solid state

(as experimentally evidenced by the crystal structures³⁰). Noteworthy is the fact that the conformation of the ribose ring is so rigid that it shows no significant sensitivity to the nature of the nucleobase. Therefore, pairs of experimentally determined²⁹ ${}^3J_{\text{HH}}$ coupling constants vs Φ_{HH} torsions³⁰ for 3',5'-cAMP, 3',5'-cGMP, and 3',5'-cUMP have been included in our dataset for the reparametrization of Haasnoot–Altona's Karplus equation.

(b) We have also incorporated ${}^3J_{\text{HH}}$ vs Φ_{HH} data for two conformationally constrained carbocyclic nucleosides, i.e., 1',6'-methano carbocyclic thymidine (**7**) and its 4',6'-counterpart (**8**). X-ray crystallography data^{6,31} show that the bicyclic skeleton adopts a boatlike conformation both in **7** (C3'-exo) and **8** (C2'-exo). The solid-state structures of **7** and **8** are fully consistent with their conformations in solution, which are based upon the interpretation of the respective ${}^1\text{H}$ NMR spectra (see the Experimental Section). However, due to possible distortion of the geometry along C1'–C6' and C4'–C6' bonds, we have excluded ${}^3J_{4'6'}$ for **7** and ${}^3J_{1'6'}$ for **8** from our dataset.

(c) The solution NMR-derived and solid-state conformations³² of [1-(3'-deoxy-3'-C,2'-O-(1-methylethylene)- β -D-ribofuranosyl)uracil] (**9**) are in good agreement, and the experimental ${}^3J_{\text{HH}}$ values are not significantly affected by the increase of temperature from 243 to 333 K, which suggests that the two constituent five-membered rings are conformationally locked. Therefore, this compound has also been used for our reparametrization.

(d) The furanose moiety in the 2',3'-cis-fused 2',3'-O-isopropylideneuridine (**10**) has a C3'-exo–C4'-endo twist conformation, as shown by its X-ray crystal structure.³³ The 2',3'-cis-fused 2',3'-O-isopropylideneadenosine (**11**) crystallizes³⁴ under two forms, molecules A and B. Whereas the sugar is nearly planar in molecule A, it is puckered in an unusual ${}^3\text{T}^4$ twist conformation in molecule B. The 2',3'-cis-fused 2',3'-O-isopropylidene-guanosine (**12**)³⁵ crystallizes as an ${}^3\text{E}$ envelope. In order to determine the solution conformation of the pentofuranose moiety in **10–12**, we have recorded their ${}^1\text{H}$ NMR spectra at 278 and 358 K in ~ 5 mM D_2O solution. ${}^3J_{\text{HH}}$ extracted from these spectra are nearly temperature independent (± 0.2 Hz), which suggests that the NMR structure is frozen (see the Experimental Section).

(e) The furanose moiety in 2,2'-O-anhydro-1- β -D-arabinofuranosyluracil (**13**) is also conformationally constrained (C3'-exo), both in the solid state³⁶ and in solution (as evidenced by the fact that the experimentally measured ${}^3J_{\text{HH}}$ are temperature-independent [± 0.2 Hz from 278 to 358 K (see the Experimental Section)]).

(f) The pentofuranose moiety in 3',5'-O-(tetraisopropyl-1,3-disoloxanediyl)cytidine (**14**) is puckered into a typical

(30) (a) Varughese, K. I.; Lu, C. T.; Kartha, G. *J. Am. Chem. Soc.* **1982**, *104*, 3398. (b) Chwang, A. K.; Sundaralingam, M. *Acta Crystallogr., Sect. B* **1974**, *30*, 1233. (c) Coulter, C. L. *Acta Crystallogr., Sect. B* **1969**, *25*, 2055.

(31) Altmann, K.-H.; Imwinkelried, R.; Kesselring, R.; Rihs, G. *Tetrahedron Lett.* **1994**, *35*, 7625.

(32) Koole, L. H.; Wu, J.-C.; Neidle, S.; Chattopadhyaya, J. *J. Am. Chem. Soc.* **1992**, *114*, 2687.

(33) Katti, S. K.; Seshadri, T. P.; Viswamitra, M. A. *Acta Crystallogr., Sect. B* **1981**, *37*, 407.

(34) Sprang, S.; Rohrer, D. C.; Sundaralingam, M. *Acta Crystallogr., Sect. B* **1978**, *34*, 2803.

(35) Mande, S. S.; Seshadri, T. P.; Viswamitra, M. A. *Acta Crystallogr., Sect. C* **1988**, *44*, 912.

(36) Delbaere, L. T. J.; James, M. N. G. *Acta Crystallogr., Sect. B* **1973**, *29*, 2905.

C3'-endo envelope in the solid state.³⁷ $^3J_{\text{HH}}$ coupling constants extracted from its ^1H NMR spectrum³⁸ suggest that the solution and X-ray structures are very similar.

(g) The X-ray crystal structure of the self-complementary DNA duplex ($\text{C}_1\text{G}_2\text{C}_3\text{G}_4\text{A}_5\text{A}_6\text{T}^*\text{T}^*\text{T}^*\text{T}^*\text{C}_9\text{G}_{10}\text{C}_{11}\text{G}_{12}$)₂, which incorporates two 6'-α-methylcarbothymidine (15) residues per strand (marked by T*), is known.¹¹ Three T* residues of this DNA duplex are puckered in S-type forms in the solid state ($P_S \sim 147^\circ$ with $\Psi_m \sim 44^\circ$), which gave average $\Phi_{\text{H-C-C-H}}$ torsions in the pentofuranose moiety, and NMR spectra provided the corresponding $^3J_{\text{HH}}$ coupling constants.⁵

(B) Results of the Reparametrization of Haasnoot–Altona's Karplus Equation (Step 9 in Scheme 2). Taking our dataset of 45 $^3J_{\text{HH}}/\Phi_{\text{HH}}$ entries, we have reparameterized the Haasnoot–Altona Karplus equation^{17b} using the Monte-Carlo module of the PROFIT program,³⁹ which is based upon a least-square fitting procedure. We have optimized P_1 – P_7 parameters in an iterative manner. The calculations resulted in the following equation

$$^3J_{\text{HH}} = 13.41 \cos^2 \Phi_{\text{HH}} - 0.98 \cos \Phi_{\text{HH}} + 1.37 + \sum_{i=1-4} \Delta\chi_{i(g)} [0.20 - 2.26 \cos^2 (\zeta_i \Phi_{\text{HH}} + 0.39 |\Delta\chi_{i(g)}|)] \quad (4)$$

where,

$$\Delta\chi_{i(g)} = \Delta\chi_{i(\alpha)} + 0.071 \sum_{j=1-4} \Delta\chi_j (\beta \text{ substituent})$$

The χ^2 value for the fitting of the experimental Φ_{HH} vs $^3J_{\text{HH}}$ data using eq 4 is 7.2 Hz,² which corresponds to an rms error of 0.40 Hz. For comparison, the rms error of the original Haasnoot–Altona equation with conventional nucleosides was in the range 0.36–0.51 Hz, depending upon the substitution patterns of H–C–C–H fragments (0.48 Hz in the case where all H–C–C–H fragments are considered together for a common set of parameters). With the help of our new Karplus-type equation (eq 4), the difference between the experimental and calculated $^3J_{\text{HH}}$ couplings, ΔJ_{max} , was below 0.5 Hz for 40 data points and in the range from 0.8 to 1.3 Hz for five data points. It should also be noted that in our approach we have a common equation for all H–C–C–H fragments. Moreover, the small P_7 value indicates the reduced influence of β-substituents. Therefore, for practical reasons, β-substituents may even be excluded when the determination of the electronegativities of the substituents is performed. The plots in Figure 5 show examples of Karplus curves built using the combination of coefficients of eq 4. It may be seen from these plots that the experimental ($\Phi_{\text{H-C-C-H}}$, $^3J_{\text{HH}}$) pairs lie very close to the theoretically calculated Karplus curves. A plot (Figure 6) of experimental versus calculated (with eq 4) $^3J_{\text{HH}}$ shows a straight line with a correlation coefficient of 0.99.

(C) The Assessment of Conformations of 1–3 Using PSEUROT Based on Eq 4 (Steps 3b–5b). We used our new set of P_1 – P_7 parameters of eq 4 in the PSEUROT program (version 3B) (steps 3b – 5b in

Scheme 2) to compare the resulting geometries for the cyclopentane ring in 1–3 with those of the previously estimated geometries using the original set of parameters of the Haasnoot–Altona Karplus-type equation (i.e., steps 3a – 5a in Scheme 2).

We have examined the conformational hyperspace of geometries that may be adopted by the cyclopentane rings in 1–3 using the same procedure as that described in section IIID (ii), i.e., by constraining the geometry of the minor pseudorotamer and scanning Ψ_m values. The average P and Ψ_m from the best results of our new sets of PSEUROT optimizations are given in Table 4, which shows that the cyclopentane rings in 1–3 adopt almost exclusively a $^0\text{E} - ^2\text{T}_1$ range ($105^\circ < P < 140^\circ$, $34^\circ < \Psi_m < 40^\circ$) of conformations (see also Table 3 for the details of all pseudorotational analyses).

The comparison (step 11 in Scheme 2) of the NMR-PSEUROT geometries derived from the calculations based upon Haasnoot–Altona's original equation vs our reparameterized Karplus-type equation shows that the end result of the analyses is very comparable in terms of phase angle and puckering amplitude for the cyclopentane rings in 1–3 (Table 3): ($35^\circ < P [^3\text{T} - ^0\text{T}] < 65^\circ$, $35^\circ < \Psi_m < 45^\circ$) \Leftrightarrow ($128^\circ < P [^1\text{E} - ^2\text{T}_1] < 140^\circ$, $34^\circ < \Psi_m < 38^\circ$) for 1, ($330^\circ < P [^1\text{T} - ^3\text{E}] < 10^\circ$, $35^\circ < \Psi_m < 45^\circ$) \Leftrightarrow ($105^\circ < P [^0\text{T}] < 116^\circ$, $34^\circ < \Psi_m < 39^\circ$) for 2 and ($340^\circ < P [^2\text{E} - ^3\text{T}] < 40^\circ$, $35^\circ < \Psi_m < 45^\circ$) \Leftrightarrow ($118^\circ < P [^1\text{E}] < 127^\circ$, $35^\circ < \Psi_m < 40^\circ$) for 3.

It may, however, be noted that the set of PSEUROT analyses performed using our reparameterized Karplus-type equation have given smaller rms error by ≤ 0.14 Hz and smaller ΔJ_{max} by ≤ 0.5 Hz than those using the original parameter set from Haasnoot–Altona (see Table 3).^{17b}

(VII) Determination of the Preferred Conformation around the γ Torsion Angle from $^3J_{4'5'}$ and $^3J_{4'5''}$ in 1–3. The preferred conformation, in aqueous solution, of the exocyclic 5'-substituent around the C4'–C5' bond [i.e., γ torsion defined by (O5'–C5'–C4'–C3')] in 1–3 was derived from the interpretation of the time-averaged $^3J_{4'5'}$ and $^3J_{4'5''}$ couplings in terms of a dynamic three-state equilibrium between γ^+ , γ^- , and γ^t staggered rotamers, by adapting the published methodology⁴⁰ to the case of our carbocyclic nucleosides 1–3 [see ref 41 and footnote e in Table 4], which show a slight preference for the γ^t (40%) rotamer.

(40) Haasnoot, C. A. G.; de Leeuw, F. A. A. M.; de Leeuw, H. P. M.; Altona, C. *Recl. Trav. Chim. Pays-Bas* **1979**, *98*, 576.

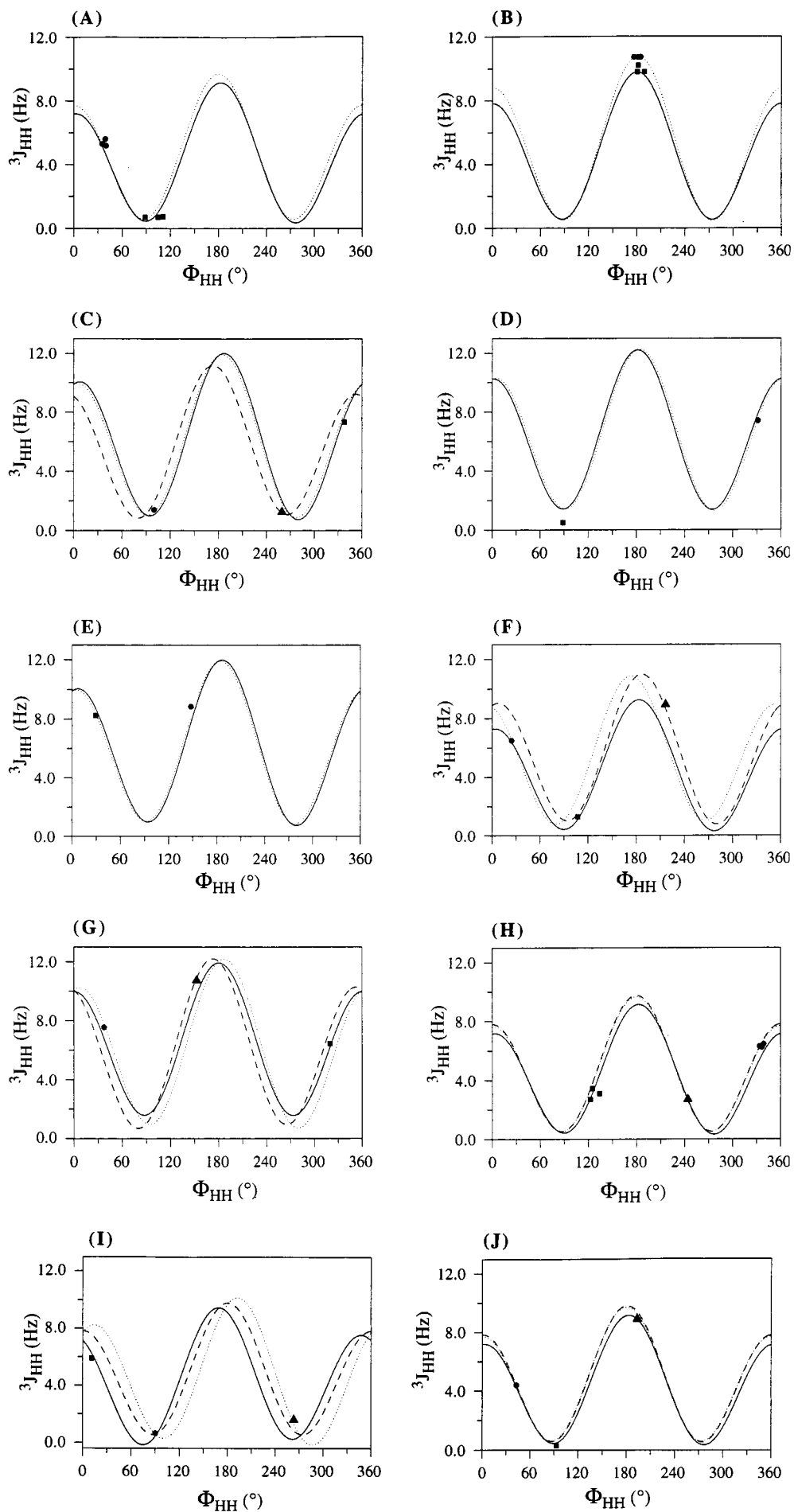
(41) The published methodology (see ref 40) used to calculate the populations of the γ^+ , γ^- , and γ^t rotamers around the C4'–C5' bond [i.e., γ is defined by: (O5'–C5'–C4'–C3')] in pentofuranosyl nucleosides has been adapted to the case of carbocyclic nucleosides 1–3 by taking into consideration the followings: (i) In contrast with the case of pentofuranosyl nucleosides, there are only a few X-ray crystal structures known for carbocyclic nucleosides; therefore, it was not possible to calculate the average values of the γ torsion angle in the pure γ^+ , γ^- , and γ^t conformers from the perusal of this statistically unrepresentative dataset. Hence, we have assumed perfect trigonal symmetry around C4'–C5' torsion in 1–3 since there is no substituent that diminishes the aliphatic similarity in those parts of the molecules (i.e., $\gamma = 60^\circ$, -60° and 180° in the γ^+ , γ^- , and γ^t rotamers, respectively). (ii) The change of the electronegativity of C6' in carbocyclic nucleosides 1–3 compared with O4' in pentofuranosyl nucleosides has been accounted for when calculating, for each of the pure γ^+ , γ^- , and γ^t rotamers, $^3J_{4'5'}$ and $^3J_{4'5''}$ by substituting the suitable values of γ (see i) into the Karplus-type equation developed by Altona et al. (ref 40).

(42) Rosemeyer, H.; Tóth, G.; Golankiewicz, B.; Kazimierczuk, Z.; Bourgeois, W.; Kretschmer, U.; Muth, H.-P.; Seela, F. *J. Org. Chem.* **1990**, *55*, 5784.

(37) Verdegaal, C. H. M.; De Kok, A. J.; Westerink, H. P.; van Boom, J. H.; Romers, C. *Acta Crystallogr., Sect. B* **1981**, *37*, 1924.

(38) Robins, M. J.; Wilson, J. S.; Sawyer, L.; James, M. N. G. *Can. J. Chem.* **1983**, *61*, 1911.

(39) PROFIT II 4.1, Quantum Soft, Postfach 6613, CH-8023 Zürich, Switzerland, 1990.



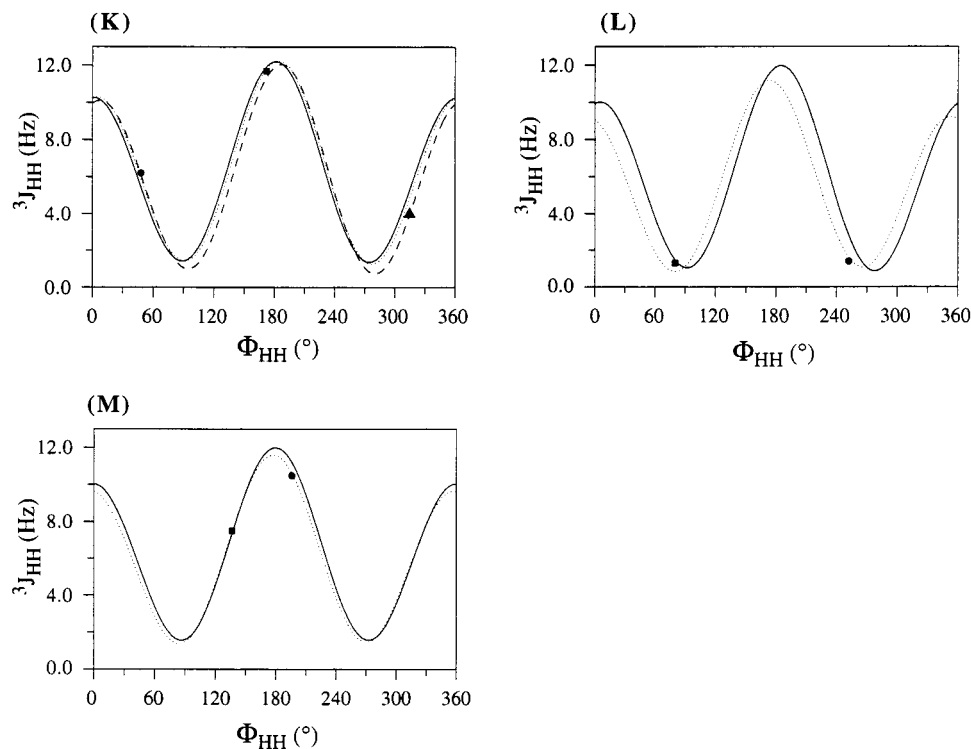


Figure 5. Plots of the calculated change of vicinal $^3J_{\text{HH}}$ as function of Φ_{HH} constructed using eq 4 for various H-C-C-H substitution patterns in **4–15** (section VIB). For each plot, the experimental $^3J_{\text{HH}}$ vs Φ_{HH} pairs are shown by the symbols denoted in parentheses in the corresponding panels. (A) $^3J_{1'2'}$ vs $\Phi_{1'2'}$ (—, ■) and $^3J_{2'3'}$ vs $\Phi_{2'3'}$ (···, ●) for **4–6**. (B) $^3J_{3'4'}$ vs $\Phi_{3'4'}$ (—, ■) and $^3J_{4'5'}$ vs $\Phi_{4'5'}$ (···, ●) for **4–6**. (C) $^3J_{2'3'}$ vs $\Phi_{2'3'}$ (—, ■), $^3J_{2''3''}$ vs $\Phi_{2''3''}$ (···, ●) and $^3J_{3'4'}$ vs $\Phi_{3'4'}$ (---, ▲) for **7**. (D) $^3J_{1'2'}$ vs $\Phi_{1'2'}$ (—, ■) and $^3J_{1'2''}$ vs $\Phi_{1'2''}$ (···, ●) for **8**. (E) $^3J_{2'3'}$ vs $\Phi_{2'3'}$ (—, ■) and $^3J_{2''3''}$ vs $\Phi_{2''3''}$ (···, ●) for **8**. (F) $^3J_{1'2'}$ vs $\Phi_{1'2'}$ (—, ■), $^3J_{2'3'}$ vs $\Phi_{2'3'}$ (···, ●) and $^3J_{3'4'}$ vs $\Phi_{3'4'}$ (---, ▲) for **9**. (G) $^3J_{3\text{Hc}}$ vs $\Phi_{3\text{Hc}}$ (—, ■), $^3J_{\text{HcHa}}$ vs Φ_{HcHa} (···, ●) and $^3J_{\text{HcHb}}$ vs Φ_{HcHb} (---, ▲) for **9**. (H) $^3J_{1'2'}$ vs $\Phi_{1'2'}$ (—, ■), $^3J_{2'3'}$ vs $\Phi_{2'3'}$ (···, ●) and $^3J_{3'4'}$ vs $\Phi_{3'4'}$ (---, ▲) for **10–12**. (I) $^3J_{1'2'}$ vs $\Phi_{1'2'}$ (—, ■), $^3J_{2'3'}$ vs $\Phi_{2'3'}$ (···, ●) and $^3J_{3'4'}$ vs $\Phi_{3'4'}$ (---, ▲) for **13**. (J) $^3J_{1'2'}$ vs $\Phi_{1'2'}$ (—, ■), $^3J_{2'3'}$ vs $\Phi_{2'3'}$ (···, ●) and $^3J_{3'4'}$ vs $\Phi_{3'4'}$ (---, ▲) for **14**. (K) $^3J_{1'2'}$ vs $\Phi_{1'2'}$ (—, ■), $^3J_{1'2''}$ vs $\Phi_{1'2''}$ (···, ●) and $^3J_{2'3'}$ vs $\Phi_{2'3'}$ (---, ▲) for **15**. (L) $^3J_{2'3'}$ vs $\Phi_{2'3'}$ (—, ■) and $^3J_{3'4'}$ vs $\Phi_{3'4'}$ (···, ●) for **15**. (M) $^3J_{4'6'}$ vs $\Phi_{4'6'}$ (···, ■) and $^3J_{1'6'}$ vs $\Phi_{1'6'}$ (···, ●) for **15**.

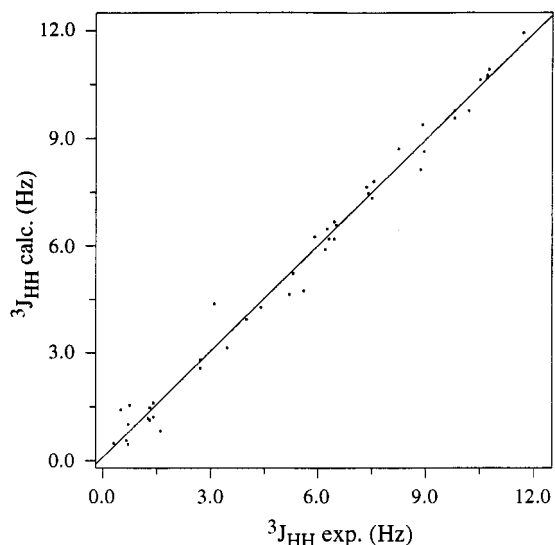


Figure 6. Correlation plot of 45 experimental $^3J_{\text{HH}}$ vs the corresponding $^3J_{\text{HH}}$ calculated with eq 4. The straight line has been fitted, and the correlation coefficient came out to be 0.99.

Conclusion

We have herein shown for the first time that the hypothesis of the two-state pseudorotational equilibrium can be used to describe the conformation of the cyclopentane ring of a carbocyclic nucleoside such as aristeromycin (**1**) and in its 2'-deoxy (**2**) and 3'-deoxy (**3**) coun-

terparts. Pseudorotational analyses, using the program PSEUROT, of $^3J_{\text{HH}}$ couplings extracted from ^1H NMR spectra recorded at various temperatures in D_2O showed that the constituent cyclopentane ring in **1–3** adopts preferentially a puckered ($105^\circ < P < 140^\circ$, $34^\circ < \Psi_m < 40^\circ$) form in solution. This result was not in agreement with that of the X-ray structure of aristeromycin hydrobromide, which exhibits an ^0E envelope conformation ($P = 89^\circ$, $\Psi_m = 41^\circ$) for the cyclopentane ring. The comparison of the NMR conformation of the cyclopentane ring of aristeromycin in neutral solution and its aglycon-protonated form in the solid state is indeed valid due to the absence of $\text{O}4'$ oxygen (and the resulting lack of anomeric effect) in the carbocyclic moiety in nucleosides **1–3**. This was also clearly evident by the pD -independent coupling constants observed for **1–3**.

That almost identical solution geometries were derived independently from ours and Haasnoot–Altona's Karplus equation shows the high confidence that can be placed in the quality of the solution structure determined in this work for aristeromycin **1**. This has also allowed us to define correctly the solution conformation of the 2'-deoxy- and 3'-deoxycyclopentane residue in **2** and **3**, respectively, using either Haasnoot–Altona's or our parametrization of the Karplus equation.

Experimental Section

^1H NMR Spectroscopy. (a) The assignment of resonances in the 1D proton spectra of **1–3** recorded in aqueous solution are based on homodecoupling and 1D-NOE difference experi-

ments. For 3'-deoxyaristeromycin (**3**), we have also confirmed the assignment using DQF-COSY and (¹H, ¹³C) HMBC (with gradients) experiments.

(b) ¹H NMR spectra of **7**, **8**, and **10–13** have been recorded in D₂O solution (5 mM concentration) at two extreme temperatures in order to investigate whether the constituent five-membered ring is conformationally locked. Assignments of the resonances have been performed using homodecoupling experiments as well as 1D-NOE difference experiments. From a first-order analysis of the spectra, the following vicinal ³J_{HH} values have been obtained (in Hz): ³J_{2'3'} = 7.3, ³J_{2''3'} = 1.2, ³J_{3'4'} = 1.1, at 288 K and ³J_{2'3'} = 7.4, ³J_{2''3'} = 1.6, ³J_{3'4'} = 1.4 at 358 K for **7**; ³J_{1'2'} ≤ 0.5, ³J_{1'2''} = 7.3, ³J_{2'3'} = 8.2, ³J_{2''3'} = 9.0 at 278 K and ³J_{1'2'} ≤ 0.5, ³J_{1'2''} = 7.5, ³J_{2'3'} = 8.2, ³J_{2''3'} = 8.9 at 358 K for **8**; ³J_{1'2'} = 2.6, ³J_{2'3'} = 6.4, ³J_{3'4'} = 3.6 at 278 K and ³J_{1'2'} = 2.8, ³J_{2'3'} = 6.5, ³J_{3'4'} = 3.7 at 358 K for **10**; ³J_{1'2'} = 3.6, ³J_{2'3'} = 6.2, ³J_{3'4'} = 2.5 at 278 K and ³J_{1'2'} = 3.3, ³J_{2'3'} = 6.3, ³J_{3'4'} = 2.9 at 358 K for **11**; ³J_{1'2'} = 3.0, ³J_{2'3'} = 6.3, ³J_{3'4'} = 2.9 at 278 K and ³J_{1'2'} = 3.0, ³J_{2'3'} = 6.3, ³J_{3'4'} = 3.0 at 358 K for

12; ³J_{1'2'} = 6.0, ³J_{2'3'} = 0.6, ³J_{3'4'} = 1.7 at 278 K and ³J_{1'2'} = 5.8, ³J_{2'3'} = 0.7, ³J_{3'4'} = 1.7 at 358 K for **13**. Note that in order to build our data set of (³J_{HH} vs Φ_{HH}) pairs (Table 5) used for the reparametrization of the Karplus-type equation (eq 4) we have also taken into account the errors inherent to the measurements of the experimental coupling constants (±0.1 Hz).

Acknowledgment. We thank the Swedish Natural Science Research Council (NFR), Swedish Board for Technical Development (NUTEK), and Swedish Engineering Research Council (TFR) for generous financial support. Thanks are due to the Wallenbergstiftelsen, Forskningsrådsnämnden, and University of Uppsala for funds for the purchase of 600 and 500 MHz Bruker DRX NMR spectrometers.

JO980364Y